LIMNOLOGY
and
OCEANOGRAPHY

ASLO

Limnol. Oceanogr. 65, 2020, 1116–1135

doi: 10.1002/lno.11438

Carbon release and transformation from coastal peat deposits controlled by submarine groundwater discharge: a column experiment study

Matthias Kreuzburg,[1*] **Fereidoun Rezanezhad**,[2] **Tatjana Milojevic**,[2] **Maren Voss**,[1] **Lennart Gosch**,[3] **Susanne Liebner**,[4] **Philippe Van Cappellen**,[2] **Gregor Rehder**[1]

[1]Leibniz Institute for Baltic Sea Research, Warnemünde, Germany
[2]Ecohydrology Research Group and Water Institute, Department of Earth and Environmental Sciences, University of Waterloo, Waterloo, Ontario, Canada
[3]Faculty of Agricultural and Environmental Sciences, University of Rostock, Rostock, Germany
[4]GFZ German Research Centre for Geosciences, Section 3.7: Geomicrobiology, Potsdam, University of Potsdam, Institute of Biogeochemistry and Biology, Potsdam, Germany

Abstract

Although the majority of coastal sediments consist of sandy material, in some areas marine ingression caused the submergence of terrestrial carbon-rich peat soils. This affects the coastal carbon balance, as peat represents a potential carbon source. We performed a column experiment to better understand the coupled flow and biogeochemical processes governing carbon transformations in submerged peat under coastal fresh groundwater (GW) discharge and brackish water intrusion. The columns contained naturally layered sediments with and without peat (organic carbon content in peat 39 ± 14 wt%), alternately supplied with oxygen-rich brackish water from above and oxygen-poor, low-saline GW from below. The low-saline GW discharge through the peat significantly increased the release and ascent of dissolved organic carbon (DOC) from the peat ($\delta^{13}C_{DOC}$ − 26.9‰ to − 27.7‰), which was accompanied by the production of dissolved inorganic carbon (DIC) and emission of carbon dioxide (CO_2), implying DOC mineralization. Oxygen respiration, sulfate (SO_4^{2-}) reduction, and methane (CH_4) formation were differently pronounced in the sediments and were accompanied with higher microbial abundances in peat compared to sand with SO_4^{2-}-reducing bacteria clearly dominating methanogens. With decreasing salinity and SO_4^{2-} concentrations, CH_4 emission rates increased from 16.5 to 77.3 μmol m^{-2} d^{-1} during a 14-day, low-saline GW discharge phase. In contrast, oxygenated brackish water intrusion resulted in lower DOC and DIC pore water concentrations and significantly lower CH_4 and CO_2 emissions. Our study illustrates the strong dependence of carbon cycling in shallow coastal areas with submerged peat deposits on the flow and mixing dynamics within the subterranean estuary.

Sea-level rise is considered to be one of the main impacts of climate change, with significant implications for mineralization processes within coastal wetlands (Nicholls and Cazenave 2010; Neubauer 2013; Plag and Jules-Plag 2013; Hahn et al. 2015; Wang et al. 2016). In particular, coastline retreat may cause submergence of terrestrial, organic carbon-rich peat sediments. The extent of submarine peat and the process-based impacts on carbon transformation processes and exchange of trace gases in shallow coastal areas have been poorly addressed. Sediment column experiments are powerful tools to investigate subprocesses and simulate changes of environmental and hydrological conditions. These changes are accelerated by land subsidence of peatland caused by their large-scale drainage for agricultural use. Land subsidence alters the hydrologic exchange processes across the land–sea interface (Nieuwenhuis and Schokking 1997; Hooijer et al. 2012) including changes in surficial runoff, subsurface mixing, and submarine groundwater discharge (SGD).

SGD is comprised of all flow of water from the seabed into the coastal ocean, predominantly recirculated seawater (SW), driven by wave action, density gradients, and sea-level dynamics (Robinson et al. 2007; Moore 2010; Cyberski 2011; Santos

*Correspondence: matthias.kreuzburg@io-warnemuende.de

Additional Supporting Information may be found in the online version of this article.

et al. 2012). SW-derived solutes, such as dissolved oxygen (O_2) and SO_4^{2-}, affect the mineralization of organic matter in the seabed (Mulholland 1981; Weston et al. 2011; Chambers et al. 2014; Rezanezhad et al. 2016). The minor fraction of freshwater SGD, typically in the order of 4–10% (Li et al. 1999; Burnett et al. 2006; Moore 2010), is mainly controlled by the hydraulic gradients and is often O_2 depleted and enriched in methane (CH_4) and free hydrogen (H_2) (Bugna et al. 1996; Slomp and Van Cappellen 2004; Andersen et al. 2005). Because coastal peatlands mostly exhibit low topographic relief, their hydraulic gradients and freshwater discharge into coastal areas tend to be relatively low (Barlow and Reichard 2010). Nonetheless, even in coastal regions of low elevation, SGD can reach values of up to 200 cm d^{-1} (Rapaglia 2005) and can, therefore, result in high fluxes of chemical compounds to the coastal environment. For instance, SGD-borne nitrogen fluxes can be of the same order of magnitude as those delivered by rivers (Seitzinger and Harrison 2008; Knee et al. 2010; Knee and Paytan 2012). This may be one factor, driving coastal productivity toward phosphorus limitation (Slomp and Van Cappellen 2004). In addition, SGD has been identified as a carbon source to nearshore marine environments (Bugna et al. 1996; Bussmann and Suess 1998; Schlüter et al. 2004; Porubsky et al. 2013).

Peatlands cover only 3% of the earth's surface, but they store about 20–25% of the global soil organic carbon (C_{org}) (Gorham 1995; Limpens et al. 2008; Strack 2008). Uptake and release of C_{org} are strongly controlled by the prevailing hydrological conditions (Roulet et al. 1992; Moore and Dalva 1993; Sirin and Laine 2008; Zauft et al. 2010; Wang et al. 2016). When drained, peatlands can switch from being a carbon sink to a source, emitting greenhouse gases such as carbon dioxide (CO_2) (Strack 2008). In contrast, flooded peatlands usually represent a source of atmospheric CH_4 (Gatland et al. 2014; Hahn et al. 2015), which has the second largest radiative forcing after CO_2 (Ramaswamy et al. 2001). On a global scale, the atmospheric CH_4 concentration has increased by more than 250% since 1750, contributing ~ 32% of the anthropogenic radiative forcing (Stocker et al. 2013). Global methane emissions from wetlands, coastal zones, and estuaries into the atmosphere have recently been assessed at 117.2 ± 49.7, 13, and 7 Tg CH_4 yr^{-1}, respectively (Borges et al. 2016; Zhang et al. 2017), but coastal estimates of CH_4 emissions remain highly uncertain due to a small number of studies and may indicate strong variations (Weber et al. 2019). Together, coastal zones were estimated to generate approximately 75% of the total marine CH_4 emissions to the atmosphere (Bange et al. 1994). In-field studies, CH_4 emissions of 126–134 μmol m^{-2} d^{-1} were associated with gassy sediments containing high organic carbon (Borges et al. 2016). The most abundant process of marine CH_4 production is microbial methanogenesis (Cicerone and Oremland 1988), a form of anaerobic respiration using, for example, CO_2 instead of O_2 as an electron acceptor (e.g., $CO_2 + 4H_2 \rightarrow CH_4 + 2H_2O$) to degrade dissolved organic carbon (DOC). Other pathways of methane production results from acetate degradation (e.g., $CH_3COOH \rightarrow CO_2 + CH_4$) (Deppenmeier 2002). The production of CH_4, however, is closely related to SO_4^{2-} reduction, which is the dominating metabolic process of DOC mineralization in anoxic marine sediments (Zehnder and Mitchell 1978; Gosch et al. 2019). Sulfate-reducing bacteria (SRB) are generally able to successfully outcompete methanogens during organic matter degradation (Whiticar 2002). High SO_4^{2-} concentrations also sustain anaerobic CH_4 oxidation, which provides an effective barrier, limiting the amount of sedimentary CH_4 that reaches the water column (Iversen and Blackburn 1981; Reeburgh and Alperin 1988; Jørgensen et al. 2001; Dale et al. 2008). Nevertheless, in near-coastal shallow regions, sediment-derived CH_4 may still represent a significant source of dissolved CH_4 in the water column. In 2010–2011, Borges et al. (2016) recorded an average CH_4 concentration in Belgian coastal surface water (< 15 km offshore) of 139 nmol L^{-1}, with values as high as 1128 nmol L^{-1}, presumably caused by outgassing from Pleistocene peat-containing sediments.

Peatlands along the coastal margins are also a major source of DOC to coastal and shelf areas (Freeman et al. 2001; Mulholland 2003). Currently, the majority of experimental studies considering carbon transformation processes from wetland soil focus on onshore processes (Kalbitz et al. 2000; Chambers et al. 2011; Wen et al. 2018; Säurich et al. 2019). A number of experimental approaches have identified the ionic strength of the advective pore water as an important factor controlling DOC concentrations and mobilization, where increasing ionic strength results in decreasing DOC release from organic soils and vice versa (Tipping and Hurley 1988; Limpens et al. 2008; Tiemeyer et al. 2017). Furthermore, Tiemeyer et al. (2017) reported that the production of DOC is dependent on the residence time of the pore water, showing a negative correlation between the DOC concentration and the pump rate-controlled advective pore water velocity. Previously observed positive correlations between the release of DOC from subsedimentary sources (e.g., buried peat) and CH_4 concentrations in the water column suggested a common carbon source (Aravena and Wassenaar 1993; Liu et al. 2011). Submerged organic-rich peat sediments can be found in shallow coastal waters offshore of adjoining peatlands (Delaune et al. 1994; Taffs et al. 2012; Kreuzburg et al. 2018), where marine microbial communities can be supplied by peat-derived DOC and SW-derived electron acceptors (e.g., O_2, SO_4^{2-}, NO_3^-). How these submerged peat deposits in the offshore areas contribute to coastal carbon cycling, however, are currently not well constrained.

In this study, we investigate the mobilization of peat-derived DOC and biogeochemical processes that control carbon transformations using a novel flow-through column experiment with natural sediments. During the experiment,

we imposed alternating cycles of upward flowing oxygen-depleted groundwater (GW) and downward flowing oxygen-rich brackish water. The main goal of the study was to monitor the biogeochemical processes governing carbon transformations in submerged coastal peat in the mixing zone of low-saline GW and brackish water. To the best of our knowledge, this is the first experimental study investigating DOC mobilization and mineralization processes in submerged coastal peat soil, in conjunction with the production of climate relevant trace gases, under dynamic (bidirectional) flow conditions mimicking freshwater–SW mixing in the so-termed "subterranean estuary" (Moore 1999).

Study site

The coastal peatland and nature reserve "Heiligensee and Hütelmoor" (Fig. 1) northeast of Rostock-Warnemünde (extending roughly 1.6 km in the north–south direction and 1.4 km in the east–west direction) experienced large anthropogenic disturbances. The site was drained for agricultural purposes until the 1970s (Dahms 1991; Voigtländer et al. 1996), and subsequently rewetted by freshwater for restoration of the biodiversity in the 1990s (Hübner and Gräff 2013; Hahn et al. 2015; Miegel et al. 2016). Until today, the peatland drains through an extensive channel system towards the south. In the last decades, the onshore area has been subject to a wide range of investigations, including gas emissions and the investigations of landside biogeochemical processes, hydrology monitoring programs as well as geologic surveys (Voigtländer et al. 1996; Lasak et al. 2010; Koch et al. 2014; Koebsch et al. 2015; Miegel et al. 2016; Jurasinski et al. 2018; Strehse et al. 2018; Wen et al. 2018). The beach area has been subject to beach nourishments, wooden groynes were installed to retain the sand and a dyke was constructed after several wash-over events (Kolp 1957; Voigtländer et al. 1996). The shoreline is covered by permeable heterogeneous sediments except for areas with peat deposits (Hübner and Gräff 2013; Kreuzburg et al. 2018), which are only low-permeable substratum (Gosch et al. 2019).

In a recent geological assessment of the development of the seabed (Kreuzburg et al. 2018), Holocene peat deposits with C_{org} contents of 37–53% and C/N ratios of 21.3–36.4 were found more than 90 m (areal extent: 0.16–0.2 km^2) in front of the coastline (Fig. 1). The isotopic signature of the lowermost offshore peat seems to be purely terrestrial ($\delta^{13}C$ –28.9‰) and thus no fractionation processes or contamination with marine organic carbon were detected. The outer boundary of the peat deposits roughly coincides with the offshore limit of a dynamic coast-parallel longshore bar (Kreuzburg et al. 2018). The location of shallower outcropping peat deposits in the northern coastal area coincides with temperature, salinity and bottom water CH_4 anomalies most likely originating from SGD (Jurasinski et al. 2018).

Materials and methods

Sediment sampling

Sediment cores were collected, in ~ 20 cm water depth, off the coastal nature reserve "Heiligensee and Hütelmoor" on 25 August 2017 using PVC liners measuring 60 cm in length and 7.5 cm in width. The sampling site of the cores P1, P2, and P3 (54.222139°N/12.168361°E) was characterized by submarine outcropping peat layers and was covered with ~ 20 cm of marine sand. The degree of decomposition of the peat, which according to von Post (1922) is defined by the color of the extracted pore water, was H 3–4.

The sand cores S1, S2, and S3 were collected in the south of the study site (54.2108°N/ 12.1582°E), where the coastline was covered with permeable marine sediments and peat deposits were absent along the coastline. Details of the geology have been presented in Fig. 2 in Kreuzburg et al. (2018).

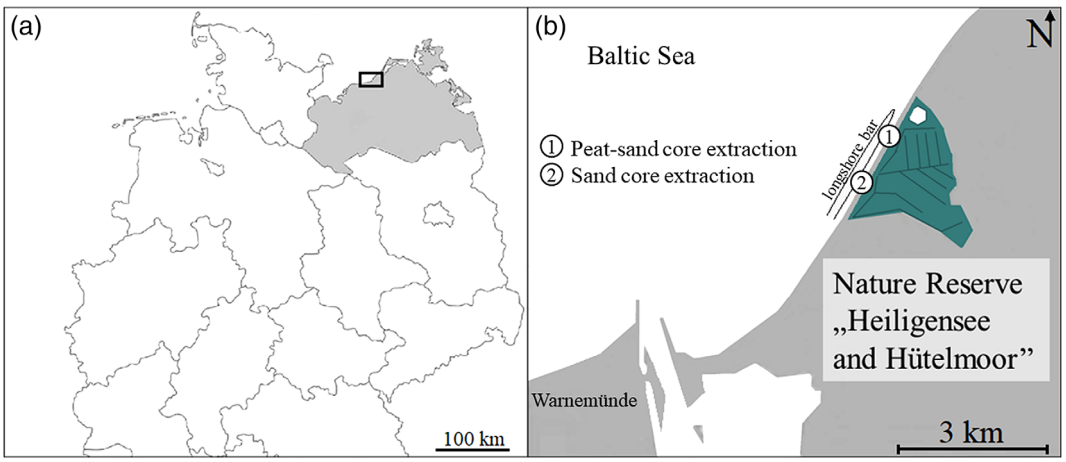

Fig. 1. Location of the study site showing (**a**) Germany with the state of Mecklenburg–Vorpommern shaded gray; the black rectangle indicates the close-up of the right side, and (**b**) location of the coastal area near Rostock-Warnemünde where sediment cores were collected in front of the nature reserve "Heiligensee and Hütelmoor" and a rough position and shape of a coast parallel longshore bar.

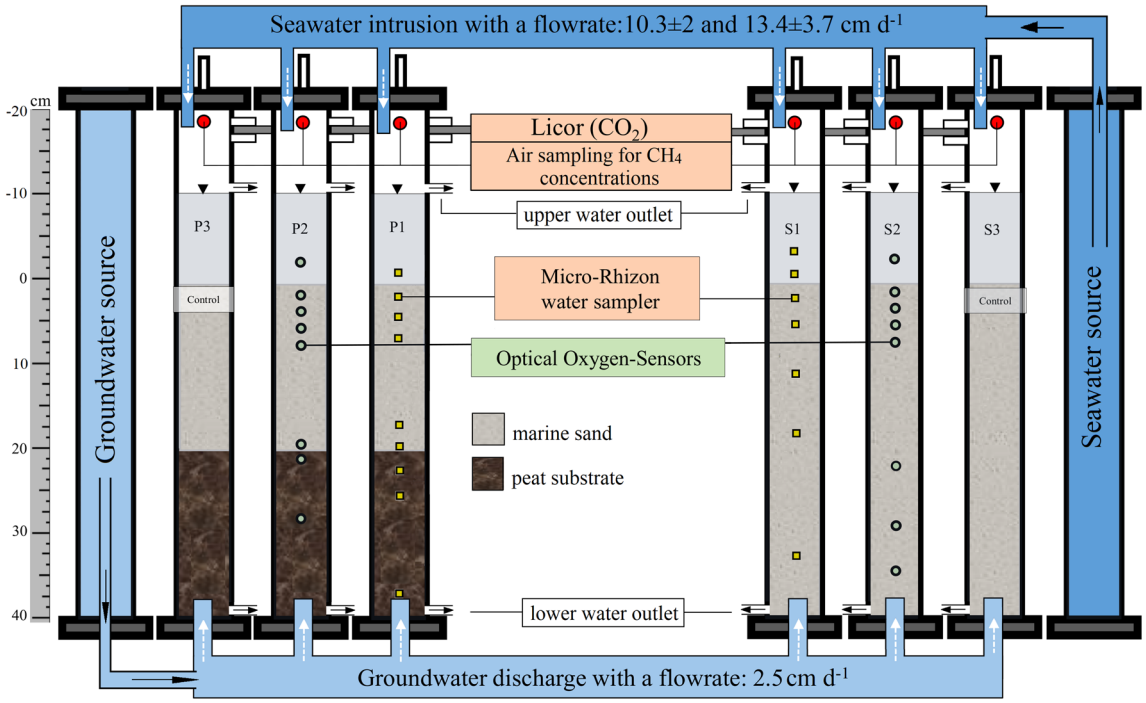

Fig. 2. Schematic diagram of the controlled flow regime column system. The six sediment columns were simultaneously and alternatingly exposed to advective flow with artificial SW from the top (outflow at the bottom) and artificial GW from the bottom (outflow near the top). Intrusive measuring devices were installed for pore water sampling (P1/S1) and optical oxygen monitoring (P2/S2). See also Fig. S1.

One core from each site was kept as a reference to compare geochemical parameters of initial and altered conditions. In order to ensure similarity of the four replicates, cores were taken within an area of < 0.25 m^2. Immediately after sampling, the cores were sealed at the top and bottom with gastight and watertight endcaps and transported to the laboratory, where they were stored at 4°C with supernatant water. Within 9 d of extraction the cores where drained, packed in a cryobox and transported via airfreight to the University of Waterloo, Canada. Visual inspection showed that the sediment sequence of the cores remained intact, but slight changes in sediment deposition could not be excluded. In the laboratory at the University of Waterloo, Canada, the sediment cores were unsealed to prevent complete anoxia and stored at 4°C for additional 16 d until the cores were installed in the experimental setup. Modifications in microbial communities and abundances, as well as redox conditions, likely occurred after transportation and storage. However, the initial microbial and redox conditions were not recorded, therefore comparison to natural conditions is limited.

Column experiment setup and instrumentation

The experiment setup included eight columns (six for sediment cores and two for water storage) made of transparent acrylic glass and matching the sediment core size. The water flow velocity through all cores was controlled by a computer-controlled pump (CAT-Multichannel-Pump Tower II, Fig. 2, Supporting Information Fig. S1). A mostly similar column system was formerly described by (Rezanezhad et al. 2014), but has been specifically refined for the variable water flow regimes in this study. In contrast to Rezanezhad et al. (2014), water of different salinities (GW, SW) was pumped through the marine sediment cores in two directions (alternating upward and downward) and discharged at the opposing end. Furthermore, the water level was kept constant and sediments were fully water saturated. The water level above all sediment columns was ~ 10 cm to approximate shallow water conditions. The lower half of three of the six 40-cm long columns was filled with naturally layered submerged peat sediments, which were overlain by marine sand. The other three cores only contained marine sand. For both sediment types, one column (P1/S1) was used to sample pore water for solute analysis, one column (P2/S2) was used for monitoring of the vertical aqueous oxygen distribution, and one column was used as a control for additional measurements of the gas fluxes and to compare pore water solute concentrations (P3/S3). The emissions of CH_4 and CO_2 were measured in all six cores.

The columns were filled from the bottom by a custom-made lifting jack and wrapped in tinfoil to prevent subsedimentary photosynthetic activity. Three of the columns were filled with 40 cm peat–sand cores containing ~ 20 cm of sand at the top. The other three columns were filled with 40-cm sand cores. The top and bottom of the columns were closed with acrylic endcaps that had O-rings lining the inner

rims to form tight seals. A filter membrane (Soil Measurement Systems, LLC, bubbling pressure: 600 mbar) closed off the bottom of the column and a nylon mesh (Soil Measurement Systems, LLC, bubbling pressure: 32 mbar) was placed on top of the filter membrane. For each column, three steel rods connected the acrylic top and bottom endcaps and were secured with bolts. The sediment columns were connected to the water storage columns with chemically resistant polyurethane tubing. In order to completely replace the air-filled pore space with water, the initial filling was conducted from the bottom with artificially produced GW (*see* "Chlorinity and conductivity" section) for 3 d at a rate of 0.3 mL min^{-1}. The total headspaces above the sediment surface were partly filled with water in the amount of ~ 888 cm^3 in Columns P1, P2, and P3 and ~ 1002 cm^3 in Columns S1, S2 and S3, respectively. All columns contained an air-filled headspace volume of ~ 478 ± 57 cm^3 (mean ± SD) above the water.

The storage columns were filled with artificial SW and fresh GW, which were continuously sparged with air and argon gas, respectively, with the latter intended to ensure oxygen-depleted conditions (details of the GW and SW compositions are given in "Chlorinity and conductivity" section). The columns were incubated at 24 ± 2°C during the entire course of the experiment. Each sediment column had 18 lateral ports (1/8″ NPT compression fittings) equally spaced every 3 cm for pore water sampling. The ports were airtight and fitted with Teflon tape. In the following text, all depths are referenced with respect to the depth below the sediment surface. The ports of four columns (P1, P3, S1, S3) were equipped with ceramic samplers, 5 cm in length and 0.25 cm in diameter, with a filter pore size of 0.15 μm (CSS5 MicroRhizon™ samplers, #19.21.23F) (Seeberg-Elverfeldt et al. 2005). The samplers were introduced horizontally into the sediment matrix, below the sediment surface, to extract pore water samples for pore water chemical and dissolved gas analyses (Fig. 2). A vacuum pump (Soil Measurement Systems, LLC, #CL-042) set at − 100 mbar was used to extract pore water through the samplers. The headspace above the stable water surface in the columns was periodically closed in order to measure sediment-derived trace gas accumulation.

Water flow regime

The upward flowing GW and downward flowing SW were set to simulate discharge and recirculation regimes through permeable coastal sediment impacted by submerged peat. The pore water flow velocities were adapted from the column experiment conducted by Tiemeyer et al. (2017), who identified a relation between DOC solution properties from organic soils, pore water velocity and composition. The height of the water table in the sediment columns was imposed using a computer-controlled, multichannel pump connected to the water storage reservoirs. The total volume of the storage columns was ~ 3.3 Liters, but the quantity of water contained varied according to flow conditions and was refilled for continuous flow. The constant ponding of the water above sediment surfaces ensured complete water saturation in the sediments and resulted from the equilibrium between the programmed pump rate and the water outflow, whereby the water in the sediment column was continuously exchanged. The GW upward flow was pump controlled at rates of 2.5 cm d^{-1} and the water-level height was limited by the water outlet ~ 10 cm above the sediment surface. The SW downward flow was controlled by the valve settings and rates were measured at 10.3 ± 2 cm d^{-1} through peat–sand cores and 13.4 ± 3.7 cm d^{-1} through sand cores. The flow ratio and flow rate were chosen to produce visible effects and changes in dissolved concentrations and volumes of the sediment column with the 50-day experiment. The ratio of GW to SW in natural shallow water conditions is typically > 1 : 10 (Li et al. 1999; Burnett et al. 2006).

During the different flow regimes, the water was discharged on the opposite side of the inflow. Flow direction and water type were adjusted using valves settings. The level of the water table in the soil columns fluctuated between 7.5 and 10 cm above the soil surface, respectively.

Coastal aquifers can be strongly depleted in oxygen (Bugna et al. 1996; Andersen et al. 2005), while shallow water along the shoreline is saturated with oxygen due to constant mixing with the atmosphere. To imitate similar conditions, argon gas was used to deoxygenate the GW and air from the laboratory was used to saturate the SW with oxygen. The artificial GW salinity was set at $S \approx 1.6$, which is slightly lower than measured values in the field ($S \approx 3$), but chosen in order to achieve a better differentiation of the end-member concentrations. The salinity of artificial SW is based on highest salinity measured ($S \approx 18$) along the shoreline of the study site (all observations from 2017). The salinity-based chloride (Cl^-) concentrations were 882 ± 66 mg L^{-1} (range: 806–1015) for GW and 8666 ± 407.1 mg L^{-1} (range: 7987–9577) for SW. Chloride was used as a conservative tracer to describe physical transport behavior and as a measure of salinity with $S = 0.00180665 \times Cl^-$ mg L^{-1} (Lyman 1969). The ratio of the other elements to chloride was based on SGD surveys in Kiel Bay, Baltic Sea in 2015 (unpublished data). Although the salinity of the Baltic Sea is largely described, there are lack of stoichiometric data on shallow shorelines and coastal aquifers. For ionic composition, *see* Table 1. All six columns were fed with SW and GW, from identical water reservoirs for the 50 d-period of the experiment.

Analytical methods

CH_4 and CO_2 flux at the water–headspace interface

The water/headspace gas flux, F_{gas}, of each column was obtained by measuring the change in gas concentration over time in the headspace after closure from the laboratory atmosphere, according to Eq. 1:

$$F_{gas} = \frac{dC_{gas}}{dt}\frac{V}{A}\frac{P}{RT}, \quad (1)$$

where dC_{gas}/dt describes the changing gas concentration (ppm) over time, V (m^3) is the volume of the headspace, and A (m^2) is the exposed water surface area. P is the atmospheric

Table 1. Composition of artificial GW and artificial SW used in the experiment.

Component (mmol L^{-1})	SO_4^{2-}	Cl^-	Na^+	Ca^{2+}	Mg^{2+}	K^+	HCO_3^-	PO_4^{3-}	NH_4	NO_3^-	SiO_2	Salinity
SW	13.2	259	223	5.2	25	4.6	2.5	0.0005	0.002	0.004	0.009	17.8
GW	0.2	29	17.4	4.2	1.6	0.37	0.37	0.02	0.0002	0.007	0.07	1.6

pressure (Pa), R is the gas constant (8.314 Pa m^3 K^{-1} mol^{-1}), and T is the absolute temperature (°K). To avoid uncontrolled gas accumulation and to minimize evaporative losses from the sediments over time, the air-filled headspaces of the sediment columns were continuously flushed with water-saturated air by passing the air through a water-filled vial. In order to determine the gas emissions from the aqueous phase into the headspace, the air ventilation was stopped. Fluctuations of the headspace volumes were taken into account in every gas flux measurement.

The fluxes of CH_4 (μmol m^{-2} d^{-1}) were monitored two to three times a week from all six cores. The concentrations were determined at the beginning (t_0) and end (t_N) of incubation (24 ± 6 h) by sampling 10 mL of headspace gas using glass syringes and were measured by gas chromatography (GC; Shimadzu Gas Chromatograph, Model GC-2014), equipped with an advanced flame ionization detector technology and helium used as an inert carrier gas. To ensure equipment accuracy, calibration standards were measured before measurement of the samples. The concentrations of the samples were within the range of calibration. For standards, a three-point calibration was used with the following certified standard gases: Level 3 = "Praxair Canada" Certified Standard, carbon dioxide 900 ppm, ± 2%, methane 95 ppm, ± 2%; Level 2 = "Praxair Canada," carbon dioxide 100 ppm, ± 2%, methane 9.8 ppm, ± 2%; and Level 1 = Air Liquide America Specialty Gases LLC (formerly Scott Specialty Gases)—Scotty analyzed gas, analysis by moles, ± 5%, carbon dioxide 600 ppm, methane 5 ppm. For CH_4 measurements with a standard deviation < 1% were conducted following a linear calibration through zero. In total, 6 mL of gaseous sample was injected into the gas chromatograph, 5 mL of which were used for flushing the system and the 1-mL sample loop.

The pore water samples for dissolved CH_4 were extracted in peat–sand columns from the sediment at depths of − 1 (i.e., above the sediment), 2, 5, 8, 17, 20, 23, 26, 38 cm and from the sand column at sediment depths of − 4.5, − 1.5, 1.5, 10.5 19.5, and 34.5 cm. Before sampling, 0.5 mL of water was extracted for flushing and eliminate the air-filled void in the syringe. Pore water samples of 1 mL were collected with 10-mL watertight, pretreated (HgCl = 25 μL) glass syringes (MICRO-Mate®) by connecting to the MicroRhizon water samplers. The sample volume of the pore water was determined by the weight (scale precision: 0.1 mg). Eight milliliters of helium was then added to form a headspace for gas equalization. After 2 h of equilibration time, by carefully shaking the syringe, which has been shown to strip at least 95% of CH_4 from the solution (Dillon et al., 1999) into the headspace, all samples were analyzed by GC on the same day of collection.

The water-headspace CO_2 fluxes were sampled daily by an automated multiplexer CO_2 flux measurement system (LI-8100, LI-COR Biosciences) via two lateral ports (Fig. 2). Air from the headspace above the water surface was then circulated through the infrared gas analyzer of the LI-8100 and back to the column. The CO_2 fluxes were calculated according to Eq. 1, whereas the rate (dC_{CO_2}/dt) was estimated from six consecutive 180-s observation windows spanning a 15-min time interval. Volume (m^3) is a combination of the headspace volume, tubing, and the sampling loop through which the headspace gas circulates. This method has been previously described by Rezanezhad et al. (2014). The CO_2 concentrations of LI-COR and GC were tested for comparability before the experiment (data not shown).

Pore water geochemistry

Pore water samples (8 mL per depth; peat–sand n = 134, sand n = 97 in total) were extracted from cores P1 and S1 with MicroRhizon™ samplers (Cabrera 1998; Knight et al. 1998; Seeberg-Elverfeldt et al. 2005) and were subsampled into separate vials. One milliliter of each water sample was filtered through a 0.2-μm membrane filter (polysulfone filter, Thermo Scientific) for the analysis of Cl^-, SO_4^{2-}, NO_3^-, and acetate ($C_2H_3O_2^-$) by ion chromatography (Dionex ICS-5000 with a capillary IonPac® AS18 column). To measure dissolved inorganic carbon (DIC) and DOC concentrations by using the nonpurgeable organic carbon method on a total organic carbon analyzer (Shimadzu TOC-LCPH/CPN, method detection limit (MDL) = 0.011 mM), 1 mL each was used. The DIC analyses were run on 7 mL samples by diluting the 1 mL samples and accounting the dilution factor in the final DIC results. DIC was sampled using open test tubes made of glass and were immediately sealed with parafilm and cooled until analyzation. This was the same for DOC analysis. The samples for DOC analyses were acidified with 20 μL of 1 M HCl. The range of reproducibility of the measurements for DIC and DOC were ± 5 and ± 12 μmol L^{-1}, respectively. Filtered pore water (< 1 mL) was analyzed for electrical conductivity (EC) using a WTW EC Meter (three-point calibration at 99.1, 999, 9976 μS cm^{-1}). The EC analyses were run on 15 mL samples by diluting 0.75 mL of pore water samples and accounting the dilution factor in the final results. Carbon isotopes of DOC were investigated at Day 50 in the pore water of the

peat–sand core (P1). For the analyses of $\delta^{13}C_{Doc}$, a portion of sample equivalent to 0.2 mg carbonate was removed from the sample aliquot and was injected in a 12-mL flat bottom Exetainer vial (Labco #739 W), where it was treated with orthophosphoric acid and potassium persulfate. The phosphoric acid addition converts inorganic carbonates present in the sample to CO_2 which is removed by bubbling with a helium gas stream for about 10 min (EPA SOP for DOC 2002; IsoPrime 2014). The sample was then sealed in the vial and microwaved. During heating, the persulfate oxidizes any DOC in the sample to CO_2. The CO_2 in the headspace of the sample vial was analyzed. Standards ranged from −12‰ (EIL-36—cane sugar) to −26.5‰ (EIL-35—beet sugar). Delta values obtained by dual inlet mass spectrometry (MS) calibrated with International Atomic Energy Agency (IAEA) carbonate standards and verified by Elemental Analyzer/Isotope Ratio Mass Spectrometry (EA-IRMS) analysis normalized with IAEA-CH3 (cellulose) + IAEA-CH6 (sugar), USGS-40, and USGS-41 (L-glutamic acid) (Stainton et al. 1977; St-Jean 2003). The results of the samples and all standard runs were statistically evaluated and were within the specification of ≤0.2‰.

Dissolved oxygen concentration monitoring

The sediment cores P2 and S2 were fitted with multifiber optode (MuFO) oxygen sensors to measure the dissolved O_2 concentration at regular depth intervals. The sensing ends were installed into the sediment columns. Eight were installed in the peat–sand column at 2, 5, 8, 14, 17, 20, 38 cm and above the sediment (− 1 cm), and eight were installed in the sand column, at 1.5, 4.5, 7.5, 10.5, 16.5, 31.5 cm and above the sediment (− 4.5, − 1.5 cm). The MuFO is a luminescence-based optode technique that uses optical sensors made of fiber optic cables, where each cable has one sensing tip and one imaging tip (Larsen et al. 2011). The sensor was built in-house using a sensing solution containing Pt(II) mesoTetra (pentaflourophenyl)–porphine as the lumniophore (Badocco et al. 2012). The uncoated ends were placed in front of a DSLR camera and blue LED light (447.5 nm wavelength) in a similar setup as described by Larsen et al. (2011). The emitted light was photographed every 2 h for the duration of the experiment and, following image processing using ImageJ software (Rasband 2015), the light intensity was related to the O_2 concentration through the Stern–Volmer relationship. The sensors were calibrated in water of the same composition as used in the experiment, in order to obtain the correct relation between light intensity and O_2 concentration. To evaluate optode light intensity responses as a function of salinity, calibrations for each sensor were conducted at a range of different salinities prior to the experiment.

Statistical analysis and data visualization

Statistical data analysis was performed to identify significant levels among the water flow regime under changing salinities and DOC and DIC production. Moreover, the relationship between salinity and O_2 as well as between SO_4^{2-} concentrations and CH_4 and CO_2 fluxes were statistically analyzed. Significant differences were accepted when the p value was smaller than significance level $\alpha = 0.05$. Gridding of pore water concentrations was performed in R-3.4.0 (R Foundation for Statistical Computing) within RStudio-1.0.143.

Quantification of methanogenic archaea and SRB

Genomic DNA was extracted from 0.2 to 0.3 g of duplicates of sediment or peat sample retrieved from Column P2 at the end of the experiment using a EURx GeneMatrix Soil DNA Purification Kit (Roboklon, #E3570). DNA concentrations were quantified with a Nanophotometer P360 (Implen GmbH) and Qubit 2.0 Fluorometer (Thermo Fisher Scientific). Quantitative polymerase chain reaction (qPCR) for the determination of functional gene copy numbers of methanogenic archaea and SRB was performed via SybrGreen assays on a Bio-Rad CFX instrument (Bio-Rad) as described elsewhere (Vuillemin et al. 2018; Wen et al. 2018) with slight modifications. In detail, the methyl coenzyme M reductase alpha subunit (*mcrA*) as the functional methanogenic gene was amplified with the primer combination mlas-F/mcra-R (*ggT gTM ggD TTC ACM CAR TA*/*CgT TCA TBg CgT AgT TVg gRT AgT*) with primer annealing at 60°C. The dissimilatory sulfite reductase beta subunit (*dsrB*) as a functional gene for SRB was quantified with the primers dsrB2060-F/dsrB4-R (*CAA CAT CgT YCA YAC CCA ggg*/*gTg Tag CAG TTA CCg CA*) with annealing at 62°C. Different DNA template dilutions (1 : 10, 1 : 50, 1 : 100) were tested prior to the qPCR runs to determine optimal template concentration without inhibitions through co-extracts. The 25 μL reactions contained 12.5 μL of KAPA SYBR® FAST mastermix (Life Technologies, San Francisco, CA), 0.25 μM concentrations of the primers, and 5 μL of DNA template. Data acquisition was done at 80°C to avoid quantification of primer dimers. The specificity of each run was verified through melt-curve analysis and gel electrophoresis. Only runs with efficiencies between 80% and 105% were used for further analysis. Measurements were performed in triplicate. Equimolar DNA mixtures of *Methanosarcina barkeri*, *Methanobacterium lacus*, and *Methanosarcina soligelidi* SMA21 were used for plasmid standards of *mcrA* and of Desulfovibrio vulgaris for *dsrB*.

Solid-phase geochemistry

At the end of the experimental period, all peat–sand and sand cores were drained overnight, extruded and sliced every 3 cm. The sediment slices from each depth were homogenized and separate aliquots were taken for geochemical characterization. For the latter, the samples were freeze-dried and stored at room temperature. Organic carbon contents (C_{org}) were measured after removal of carbonates with 10% HCl. The stable isotopic ratio of solid organic carbon ($\delta^{13}C$) were determined on the initial (kept as a reference) and postexperimental sediment cores. The samples were ground in an agate motor mill. Splits of 10–20 mg powdered, homogenized sample were weighed in

tin and silver containers (Nieuwenhuize et al. 1994). Stable isotope analyses on $\delta^{13}C$ were performed using an IRMS (Thermo Fisher Scientific), connected to an elemental analyzer via an open split interface (Multi EA 2000 CS). The reference gas was ultrapure CO_2 from a bottle calibrated against international standards (IAEA-C3, IAEA-C6, NBS 22) at the Leibniz-Institute for Baltic Sea Research (IOW). Calibration for carbon quantities was done with acetanilide reagent. The lab internal standard was peptone (Merck) with a standard deviation of < 0.2‰. Considering the 3-cm slice thickness, the depth data were interpreted and compared with the initial cores.

Results

Solid-phase geochemistry

Results from C, N, and $\delta^{13}C$ isotope analyses (Fig. 3) identified strong variations in elemental concentrations with depth within both the experimental cores (end) and the initial (init.) core. The experimental cores were exposed to the 50-day flow-through treatments, whereas the initial cores were kept as a reference until geochemical analysis at the end of the experiment. The stable isotope values ($\delta^{13}C$) in the peat layers were in the range of − 27.9‰ to − 26.8‰, with mean values of − 27.3‰ ± 0.3‰, and exhibited higher values in the upper 20-cm sand layer (in the range of − 25.3‰ to − 22.6‰, with a mean value of − 24.6‰ ± 1.5‰). In peat–sand columns, the mean concentration of C_{org} in the peat layers (depth below 30 cm sediment depth) was 44.2% ± 5.3% compared to 15.9% ± 20.2% in the transition layer between the peat and sand (sediment depth of 30–21 cm) and 0.04% ± 0.02% in the upper sand layer (Fig. 3). Total nitrogen was only detectable in the peat layers (a mean value of 1.5% ± 0.6%) and followed the depth distribution of C_{org} ($r^2 = 0.85$, $p = 0.007$). Here C : N ratios decreased from 29.5 ± 1.7 in the peat layer to 10.9 ± 0.2 in the transition layer (20–30 cm). In contrast, in the sand columns, the mean concentrations of C_{org}, C_{inorg}, and TN were very low or not detectable and a greater variance was observed for $\delta^{13}C$ (Fig. 3). The concentration of C_{inorg} in the peat layer and the sand on top in the peat–sand core (end.) was 6.5% ± 5.3% and 0.04% ± 0.03%, respectively, with significant differences to the peat–sand core (init.).

Aqueous-phase geochemistry

Chlorinity and conductivity

A high correlation for the salinity calculated with Cl^- and the salinity resulting from the EC was observed for peat–sand columns ($r^2 = 0.79$, $p < 0.001$, $n = 134$) and sand cores ($r^2 = 0.90$, $p < 0.001$, $n = 97$) (Fig. S2). Because Cl^- is known not to be affected by sorption processes, it was chosen as a measure of salinity (S). The highest salinities ($S > 12$) were

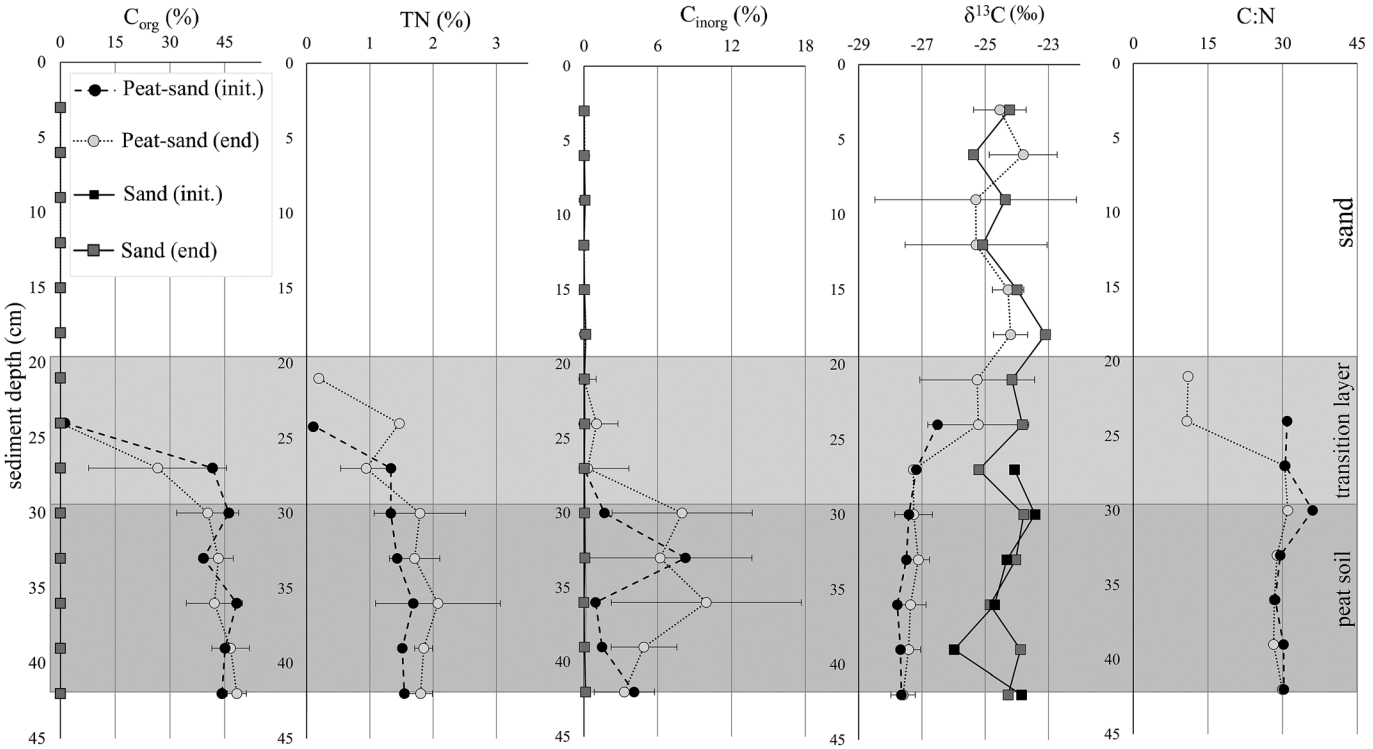

Fig. 3. Depth distribution of organic carbon contents (C_{org} %), total nitrogen (TN %), inorganic carbon (C_{inorg} %), stable isotopic signature of organic carbon ($\delta^{13}C$‰) and carbon/nitrogen ratios (C : N) in the peat-sand and sand columns from the cores after the 50 d treatment (end) and from cores in their initial state (init). Shown are mean values and standard deviation of cores of the same sediment type and represent a sediment slice of 3 cm thickness. The gray box shading indicates peat layers for the peat-sand columns. All measurements were made after the end of the experiment.

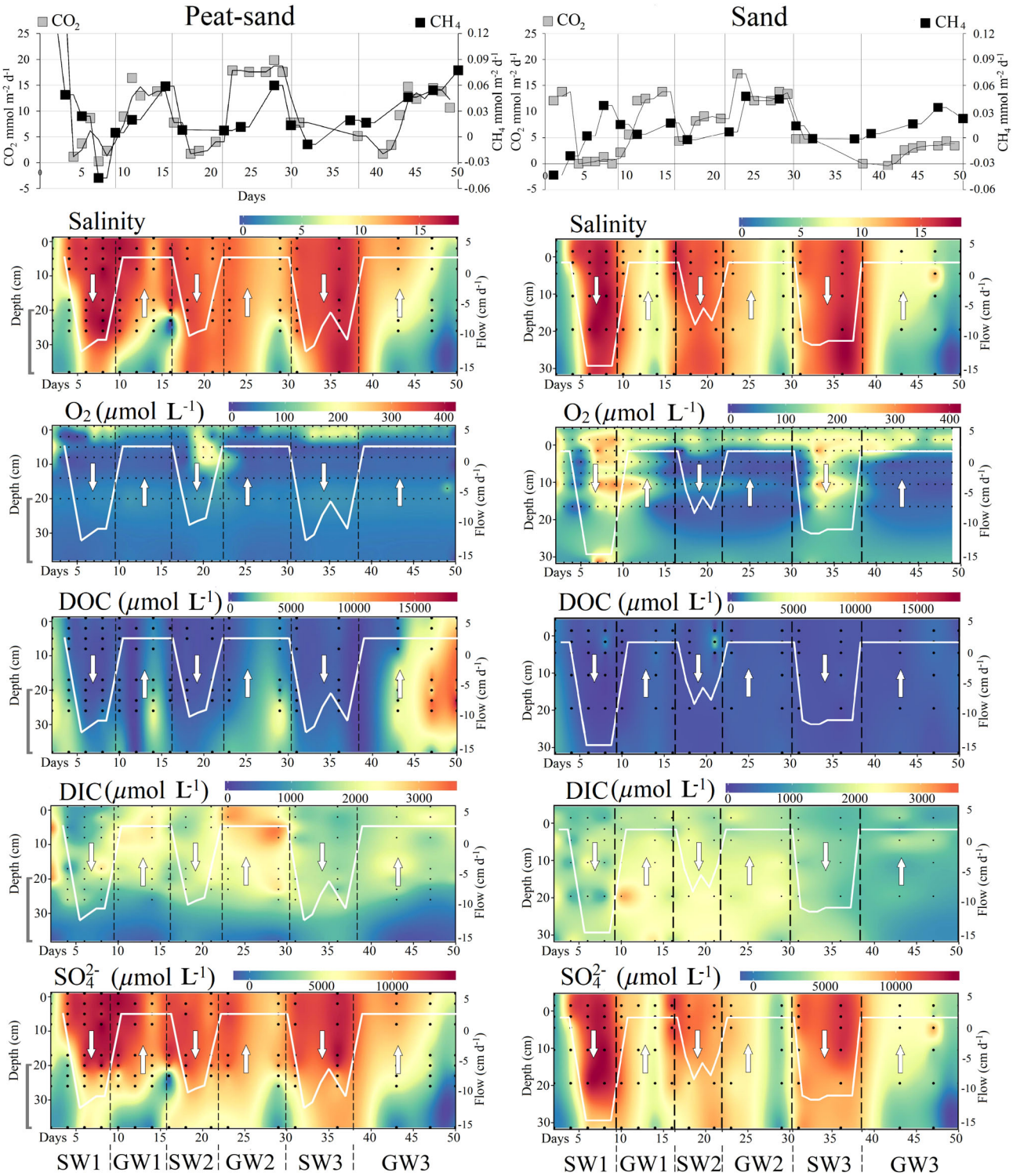

Fig. 4. The fluxes of CO_2 and CH_4 (upper graphs) derived from concentration change rates in the headspace of all columns for peat-sand (left) and sand (right). Depth distributions of aqueous concentrations of salinity, O_2, DOC, DIC and SO_4^{2-} are presented for each column set, over the 50 d of the experiment period and under GW and SW flow regimes. The white arrows show the flow direction, the white lines indicate the advective flow rates with negative values indicating downward SW flow and positive values show upward GW flow. The black dots represent the pore water sampling depths and time of sampling. The gray bracket left of the peat-sand data indicates the peat layer in the lower section (20–40 cm) of the core.

measured during the three SW cycles in the entire depths of the peat–sand and sand columns. During the GW cycles, the salinity along the column depth decreased to 6.7–9.5, and the lowest salinity ($S < 5$) was measured at the bottom of the peat–sand column during the upward GW flow after 14 d at the end of the experiment (Fig. 4).

Pore water chemistry

The dissolved oxygen (O_2) concentration in both peat–sand and sand columns varied following the SW and GW flow regimes and increased with SW intrusion phases (Fig. 4). In the peat–sand column, sediment depths > 15 cm showed oxygen concentrations of 42 ± 10.9 μmol L^{-1}, but were 70 ± 50 μmol L^{-1} in sediments above and 121 ± 29 μmol L^{-1} at the uppermost sensor in the water column. In comparison, the sand columns were entirely penetrated with oxygen. The highest O_2 concentrations (240.5 ± 67 μmol L^{-1}; range: 103–374 μmol L^{-1}) were observed at Day 7 in the upper part of the sand columns (Fig. 4) during SW downward flow regime (Fig. 4).

In both the peat–sand and the sand columns, the aqueous concentration of SO_4^{2-} showed a positive correlation (Fig. S3) with the SW downward flow events (peat–sand: r^2 = 0.85; sand: r^2 = 0.92), identifying the SW as the source of SO_4^{2-}, but showed increasing deviation with depth (Fig. 4). During the GW upward flow a significant increase in concentrations of DOC (r^2 = 0.81, $p < 0.001$) was detected with decreasing salinities in the peat–sand column. Furthermore, the increased production of DOC with advective GW upflow resulted in ascent and enrichment of DOC in the sand sediment above the peat layer (Fig. 4) and revealed acetate concentrations of 6 ± 1.2 mL L^{-1} (GW1), 8.4 ± 1.4 mL L^{-1} (GW2), and 4.6 ± 1.3 mL L^{-1} (GW3) (data not shown). With increasing salinities during SW downward flow, a significant decrease of DOC concentration in the pore water was observed. During the downward flowing SW2 phase (Day 18, Fig. 4), the O_2 concentrations strongly increased in the surface sediments. The following GW2 upward flow showed highest pore water DIC concentrations and occurred together with highest CO_2 emissions (Fig. 4) in the peat–sand cores. The final GW3 upward flow event lasted for 14 d, and strongly lowered the salinity and substantially increased the concentrations of DOC (~ 18 mmol L^{-1}) over the entire sediment core length (Fig. 4).

Stable isotopic composition of DOC

The isotopic signatures of $\delta^{13}C_{DOC}$ in P1 were 26.7‰ ± 4.5‰ with lowest values of – 26.9‰ to – 27.7‰ at salinities of $S \leq 5$. Slightly heavier $\delta^{13}C_{DOC}$ – 26.7‰ to –25.6‰ were detected at salinities $S > 5$. A linear multiple regression between $\delta^{13}C_{DOC}$, DOC, and salinity indicate a moderate adjusted determination coefficient (r^2 = 0.72) with lighter values found with higher DOC concentration and decreasing salinities (Supporting Information Figs. S4 and S5).

CO_2 and CH_4 fluxes

During GW upward flow regimes, average CO_2 fluxes were significantly higher in peat–sand (11.4 ± 5.8 mmol m^{-2} d^{-1}) and sand (6.9 ± 5.7 mmol m^{-2} d^{-1}) compared to SW downward flow regimes with 4.6 ± 3.4 mmol m^{-2} d^{-1} (peat–sand) and 3.7 ± 3.4 mmol m^{-2} d^{-1} (sand) (Fig. 4). The lowest average CO_2 fluxes of 0.5 mmol m^{-2} d^{-1} were observed in the sand cores during the SW1 down flow regime. In both sediment cores, the highest fluxes occurred during GW2 (15.7 ± 1.2 mmol m^{-2} d^{-1} in peat–sand and 12.9 ± 0.9 mmol m^{-2} d^{-1} in sand). Likewise, CH_4 fluxes reacted to the flow dynamics showing significantly higher average CH_4 fluxes during GW upward flow regimes with 35.7 ± 26.3 μmol m^{-2} d^{-1} in the peat–sand cores and 21.2 ± 16 μmol m^{-2} d^{-1} in the sand cores, compared to the SW downward flow regimes with average CH_4 fluxes of 1.5 ± 26.6 μmol m^{-2} d^{-1} peat–sand and 8 ± 15.4 μmol m^{-2} d^{-1} in the sand cores. The highest average CH_4 fluxes (32.9 ± 16.8 μmol m^{-2} d^{-1}) in the sand core were measured during GW2 and in the peat–sand cores during GW3 (48.5 ± 25.1 μmol m^{-2} d^{-1}). The longer the GW flow condition persisted, the more CH_4 was emitted (from 16.5 to 77.3 μmol m^{-2} d^{-1} during GW3) in the peat–sand cores (Fig. 4). During several SW intrusion regimes (SW1 and SW3), a reduction of the CH_4 concentrations indicate negative fluxes.

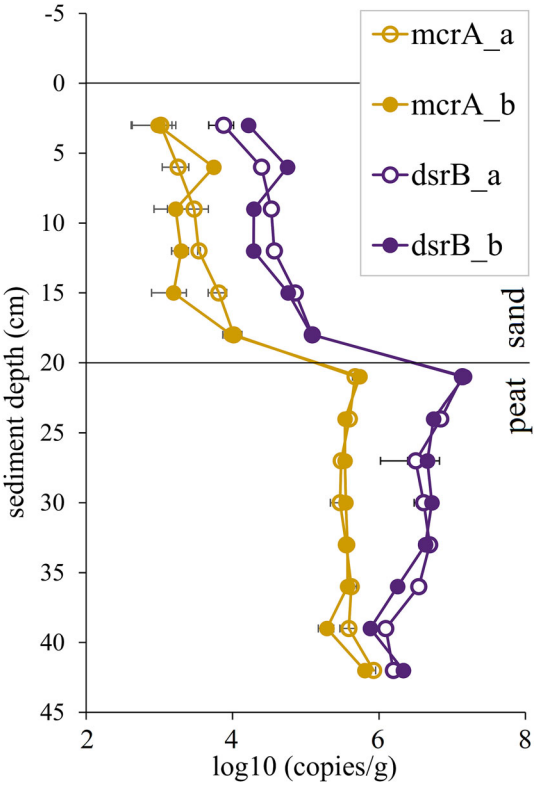

Fig. 5. Microbial abundances of methanogens and sulfate reducers. Replicates (**a**,**b**) of gene copy numbers (*mcrA, dsrB*) were measured in sediments of the peat-sand column (P2) after the experiment. The line indicates the peat–sand interface.

Abundances of methanogenic archaea and SRB

The results of the qPCR in the peat–sand column reveal significantly lower abundances of methanogens (*mcrA*) and sulfate reducers (*dsrB*) in the upper 20 cm of sand sediment (*mcrA*: $1.2 \times 10^3 \pm 1 \times 10^3$ copies g^{-1}; *dsrB*: $1.4 \times 10^4 \pm 1.2 \times 10^4$ copies g^{-1}) compared to the lower peat section (*mcrA*: $5.6 \times 10^5 \pm 2.1 \times 10^5$ copies g^{-1}; *dsrB*: 6.7 copies g^{-1}) (Fig. 5). The highest copy numbers of *dsrB* (1.9×10^7 copies g^{-1}) are detected in the transition zone (*see* Fig. 4) of highly degraded peat, whereas *mcrA* reveal highest abundances (1.02×10^6 copies g^{-1}) in the lowermost sample where peat is least decomposed. The abundances of *dsrB* are overall dominating those of the *mcrA*, while the abundance of *dsrB* declined toward the bottom section.

Discussion

Solid-phase geochemistry

A distinct shift from a terrestrial, freshwater environment (peat) to a marine saltwater environment (sand) is indicated by a sudden vertical change of the substrate at 20 cm sediment depth in the peat–sand cores (Fig. 3, Supporting Information Fig. S1). The peat layer is characterized by low C : N ratios of ~ 30 and light $\delta^{13}C$ values of approximately − 27‰. A typical enrichment in the isotopic signatures of the organic carbon toward the sand confirms a change into marine deposit conditions (Bickert 2000) and is supported by lower C : N ratios of the organic carbon source (Meyers 1997). Sediment cores without peat (S1, S2, S3) and the sandy part of the peat–sand cores have higher $\delta^{13}C$ values of − 24.3 (± 1)‰ typical for marine origin (Stein 1991). The close proximity of marine sandy sediments with peat layers induces a high downcore gradient of organic carbon of different composition and origin. Moreover, the degree of decomposition of the peat, changed from being less decomposed (*H* 3–4) in depths > 30 cm to moderately decomposed (*H* 7–8) toward the peat–sand interface (i.e., within the transition layer), coinciding with a C_{org} decrease of 99.9% (Fig. 3). These findings indicate that peat soil covered with permeable sediments is subject to decomposition, progressing from the sand–peat interface. In contrast, coastal peat deposits in > 30 cm sediment depth remained largely unaffected by SW circulation-related decomposition. This can be assumed on the basis of the content (44.2% ± 5.3%; range: 31–50%) and the isotope signature (− 27.9‰ to − 26.8‰) of C_{org} and can be explained by the low permeability of the degraded peat surface. As a result of the high C_{org} and C_{inorg} concentrations detected in the lower peat layers (> 30 cm, Fig. 3), an enhanced mineralization rate is assumed.

Advective flow regime and solute transport

Geochemical variables and fluxes in the peat–sand core and the homogenous sand core were very different. Although it was possible to generate comparable flow regimes in the two types of sediment cores by gravity driven, valve-controlled downward flow and pump-controlled upward flow, the mixing of the two salinity end-members showed clear differences assumed to be caused by the different permeabilities between the peat–sand and the sand cores. The sand cores had less constrained internal mixing compared to the peat–sand cores (Fig. 4, salinity). The mixing of GW and SW in the sand cores extended over the entire profile, resulting in a smooth vertical salinity gradient. The formation of low-saline pore water reservoirs in sediment depths > 20 cm was mostly inhibited and only formed during GW3 during Days 43–50 ($S \approx 1.6$, Fig. 4). The higher density of saline SW compared to the low-saline GW underneath may have caused density-

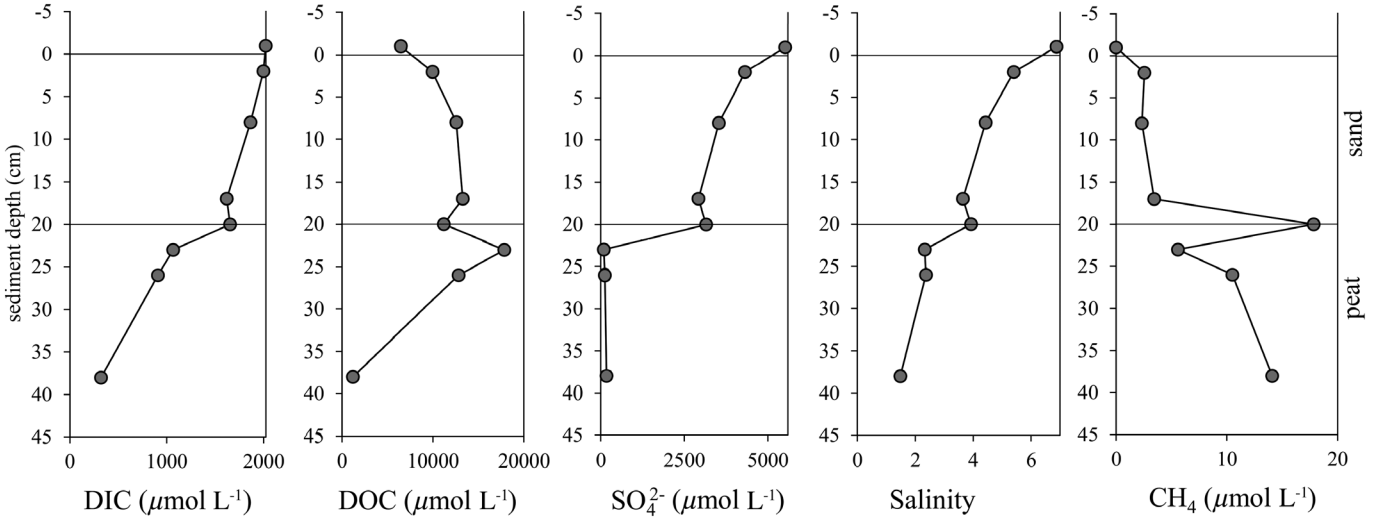

Fig. 6. Concentrations of DIC, DOC, SO_4^{2-}, CH_4 in pore water profiles of peat–sand column (P1) at the last day of the experiment (Day 50). The black line at 20 cm sediment depth indicates the peat/sand interface.

driven convection currents as described for permeable coastal sands (Robinson et al. 2007; Santos et al. 2012). In contrast, peat soils are highly complex porous media that include open and connected, dead-end, and isolated pores, where flow and convergence of GW and SW is restricted to the hydrologically active pore space (Rezanezhad et al. 2016). The solution capacity of DOC increases with decreasing conductivity (Tipping and Hurley 1988; Kalbitz et al. 2000), which has also been shown to affect the hydraulic conductivity of peat substrate (Plaut et al. 2013). In the Baltic Sea, where peat deposits and the discharge of low-saline GW are frequently observed along the coastal zones (Peltonen 2002; Schlüter et al. 2004; Kotwicki et al. 2014; Sergeev et al. 2015; Kreuzburg et al. 2018), these processes can have potential implications on the marine carbon balance. Coastal hydrodynamics in the Baltic Sea are predominantly controlled by wind conditions, and the water circulation in coastal sediments depends on the wave setup, water level, and GW recharge. Apart from a highly complex circulation pattern under in situ conditions, being, for example, not limited by vertical flow directions as in the experiment, the SW properties of the Baltic Sea (salinity, temperature, nutrient concentration) can be subject to large variations.

Carbon mineralization processes

Mobilization and transformation of DOC

Downcore concentration profiles of DIC, DOC, salinity, and SO_4^{2-} in the pore waters clearly show different slopes above and below the peat layer, indicating different processes in these substrates. Throughout the cores, salinity steadily decreases in the downcore direction (Fig. 6), while the other substances undergo production, consumption, and conversion processes. Within the organic-rich peat soil (>30 cm), pore waters were depleted in SO_4^{2-}, which indicates SO_4^{2-} reduction in the sediments above and favors CH_4 production in deeper peat layers (Figs. 6, 7, Supporting Information Fig. S2). The rate of DOC production from C_{org} appears to be primarily controlled by the conductivity of the pore water and indicates that the source of DOC is of low-saline water, resulting in an inverse relation between the concentrations of Cl^- and DOC (Fig. S4). The impact of pore water flow velocities, different flow regimes, and temperature can be relevant for DOC production from organic carbon (Tipping and Hurley 1988; Kalbitz et al. 2000; Koehler et al. 2009; Evans et al. 2012; Tiemeyer et al. 2017). In contrast to most studies, Gosch et al. (2018) observed an increase of DOC release with increasing salinities, which was explained by the specific geochemical properties of the investigated peat substrate. However, in our study, elevated concentrations of DOC and a stronger conformity of $\delta^{13}C$ values between DOC and C_{org} were observed at salinities < 5, confirming peat as the carbon source for DOC in low-salinity conditions (Fig. S5). Heavier $\delta^{13}C_{DOC}$ values were observed with increasing salinity conditions, likely a result of organic carbon degradation by SO_4^{2-} reduction (Anderson and Arthur 1983; Boutton 1991).

The upward convection of DOC with advective fluxes is obvious during GW flow regimes and is mostly pronounced during GW3 showing high concentrations (DOC ≈ 6.5 mmol L^{-1}) even in discharging surface water (Figs. 3, 5) at Day 50, which is caused by leaching of solid C_{org}. According to other studies, the effects of ionic strength on DOC release are not consistent and varies with substrate and physicochemical factors (Tipping and

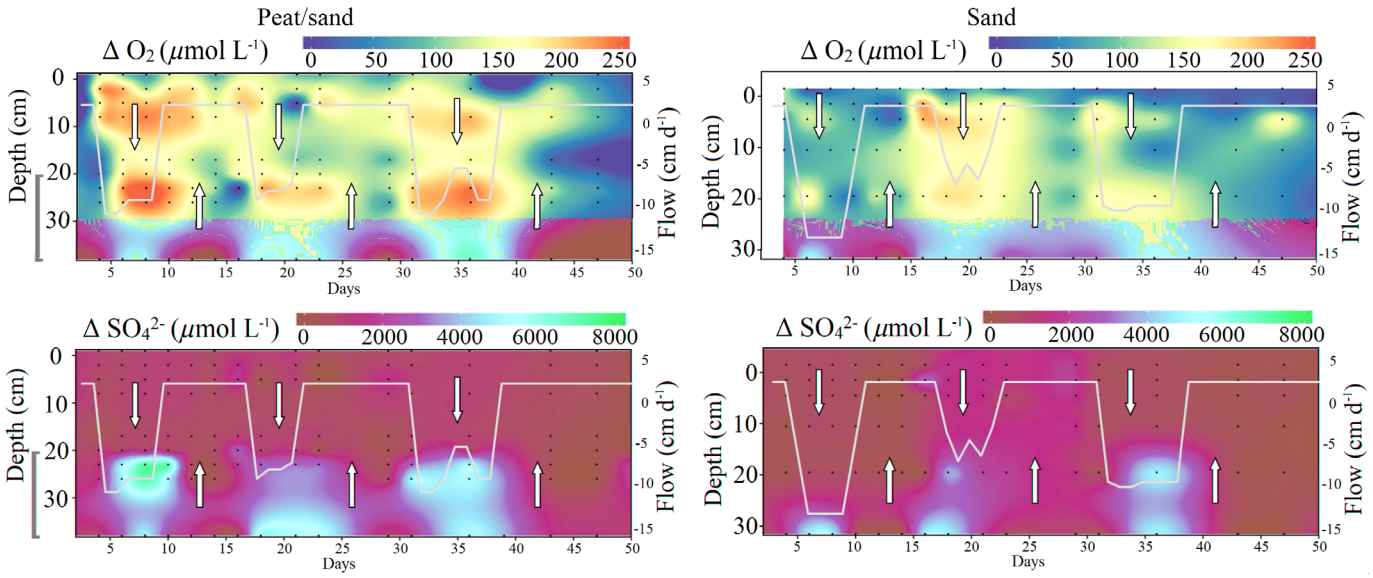

Fig. 7. Depth distribution of O_2 and SO_4^{2-} deviating from the initial end-member concentration, ΔO_2 and ΔSO_4^{2-}, presented for each column set (column P1 and S1), over 50 d of the experiment period. The gray bracket left of the peat–sand data indicates the peat layer in the lower section (20–40 cm) of the core.

Hurley 1988; Berry et al. 1990; Tiemeyer et al. 2017; Gosch et al. 2018), but the mobilization of DOC from organic sediments is apparently reduced by increasing ionic strength due to flocculation processes (Kalbitz et al. 2000). SO_4^{2-} reduction and oxic respiration are responsible for the major share of DOC oxidation in marine endobenthic environments (Bender and Heggie 1984; Henrichs and Reeburgh 1987) and we assume that this is also true for the peat-derived DOC in our experiment. Highly decomposed peat has only small quantities of organic carbon that can still be turned into decomposable DOC (Strehse et al. 2018). The peat in deeper layers exhibits significantly lower degrees of decomposition and higher C_{org} contents, thus we assume this peat may still contain significant amounts of decomposable DOC. The fate of this DOC in pore or surface waters containing mineralization-relevant substances (e.g., electron acceptors such as SO_4^{2-}, O_2) leads to the oxidation of DOC and transformation into DIC. Our results from the pore water analysis indicate the occurrence of these processes, in particular at the end of the experiment, where an increase in DIC at the peat–sand interface coincides with a decrease in DOC and a deviation between SO_4^{2-} and salinity (Fig. 6).

Previous studies have shown that with salinities $S > 10$, SO_4^{2-}-derived DOC mineralization is the preferred metabolic process, causing increased CO_2 production due to DOC mineralization (Weston et al. 2011; Chambers et al. 2014). In contrast to O_2, which is depleted in the surface sediments in our experiment (< 10 cm, Figs. 4 and 7), there is a moderate correlation between Cl^- and SO_4^{2-} (*see* "Solid-phase geochemistry" section and Fig. S3). Without any metabolic processes, the concentration of the main electron acceptors, O_2 and SO_4^{2-} in our experiment is predefined by the mixture of the two end members (SW and GW, for composition, *see* Table 1). Under the assumption that the concentration within the GW end member is negligible, used electron acceptors (ΔEA) can be directly derived from the salinity content using Eq. 2:

$$\left(\frac{EA_{max}}{Sal_{max}} Sal_{sample}\right) - EA_{sample} = \Delta EA. \quad (2)$$

This allows calculating the loss of electron acceptors (ΔEA) by calculating the difference between this "preformed" available electron acceptors (AE_{SW-GW}) and the observed AE_{Sample} at any point of the experiment for O_2 and SO_4^{2-} (Fig. 7). The data clearly indicate the higher use of electron acceptors in the peat–sand cores in comparison with the sand cores, indicating SO_4^{2-}-fueled oxidation driven by penetration of SO_4^{2-} into the decomposable peat layer. The upward advection of DOC and DIC during the GW stages leads to the increase of both parameters in the peat-overlying sands, where further oxic DOC decomposition might be partially responsible for oxygen demand and DIC increase. During phases of SW intrusion, SO_4^{2-} entering the decomposable DOC pool apparently enhances anaerobic DOC oxidation in the sediments at depth > 20 cm. Terminal electron acceptors (O_2, SO_4^{2-}) have been constantly added during SW phases of the experiment, while the solution was free of iron (Fe^{3+}) or manganese (Mn^{4+}). However, these terminal electron acceptors can be present in peat soils and fuel mineralization processes (Küsel et al. 2008; Burdige 2011). A major depletion of the terminal electron acceptors in organic-rich sediments can facilitate methanogenesis.

Depth profiling of microbial abundances (Fig. 5) supports the suggested electron acceptor utilization along the sediment column. The ratio of gene copy numbers of *dsrB* and *mcrA* increases in the peat in an upward direction, indicating SRB to be more abundant in the transition zone in which SO_4^{2-} and DOC are easily available (Fig. 5). Although gene copy numbers of *dsrB* dominate overall, the copy numbers of *mcrA* are stable across the whole peat section, suggesting their abundance does not depend on the peat characteristics nor on the increasing abundance of the sulfate reducers in an upward direction. Instead, this could be evidence that the high availability of peat-generated dissolved DOC enables the coexistence of both methanogenic and sulfate-reducing microbial communities and that their activity is subject to the changing environmental conditions. However, it cannot be excluded that the detected overlap of both groups was at least to some degree triggered by advective fluxes in the peat–sand core. The molecular data are mostly dependent on the choice of primers. Although the primers used in this study are well evaluated and have been applied for estimating the abundance of methanogens (Wen et al. 2018) and sulfate reducers (Vuillemin et al. 2018), the primers used are covering only a small diversity of microorganisms involved in the complex biogeochemical processes. However, the total abundance of microorganisms across the sediment columns has identified the peat as the favorable habitat.

Gas formation, transport, and emissions

The upward flowing GW regularly decreases the pore water salinity and thus displaces required oxidants (SO_4^{2-}) for SRB. This likely promotes anoxic DOC mineralization by methanogensis and CH_4 formation, which can be the result of fermentation of acetate (Stadtman and Barker 1949; Whiticar et al. 1986). It is further notable that in the peat–sand cores CO_2 emissions during GW1, GW2, and GW3 reached similar and constant flux rates. This may indicate a limit of mineralization activity controlled by the amount and composition of solutes present and additional, the result of anaerobic CH_4 oxidation (Reeburgh 1980).

Most pathways of microbial organic carbon oxidation, except for SO_4^{2-} reduction, are less active with increased Cl^- or HS^- concentrations (Joye and Hollibaugh 1995; Chambers et al. 2011; Luo et al. 2017). However, microbial DOC oxidation by SRB and methanogens can also coexist (Fig. 5) and may depend on availability and quality of the substrate

(Holmer and Kristensen 1994; Dar et al. 2008; Sela-Adler et al. 2017) and species-dependent metabolic traits (Ozuolmez et al. 2015). The emissions of CH_4 have been described as the residual of CH_4 production (e.g., methanogenesis) and CH_4 oxidation (e.g., aerobic and anaerobic CH_4 oxidation), and the magnitudes of CH_4 emissions can be controlled by advective transport processes (Heyer and Berger 2000). Assuming that CH_4 formation increases with DOC concentration in the absence of O_2 and SO_4^{2-}, this process is likely more relevant in peat-containing coastal sediments, where DOC production is not limited due to the solid organic carbon source. The transfer and extrapolation of CH_4 emissions observed during the experiment to the coastal area of peat-containing sediments have to be treated with caution, as coastal processes are difficult to assess and the microbial and physicochemical properties change during sampling, transport, and construction of the column setup. Although the main driver of air–water CH_4 transfer in experimental approaches is often assumed to be driven by molecular diffusion (Moore and Dalva 1993; van Winden et al. 2012), the emissions of CH_4 in shallow water can also be the result from ebullition (Ostrovsky 2003) and can be enhanced by wind and wave action interacting with coastal sediments as well as temperature and may display large spatial and temporal variabilities (Bange 2006; Upstill-Goddard 2006; Aben et al. 2017). In the case of our experiment, the advective transport of dissolved methane, forced by alternating phases of advective inflow and outflow, has a strong control on the gas flux into the water column (Fig. 4). Our mean experimental CH_4 fluxes during GW discharge ($35.7 \pm 26.3\ \mu mol\ m^{-2}\ d^{-1}$ peat–sand core; $21.2 \pm 16\ \mu mol\ m^{-2}\ d^{-1}$ sand core) were in the range of the field-based study reported by Bange et al. (1994), where they estimated an average CH_4 flux of 22–37 $\mu mol\ m^{-2}\ d^{-1}$ from the continental shelves of the Baltic Sea and the North Sea with total emissions ranging from 0.35 to 0.75 $Tg\ C\ yr^{-1}$ (Bange 2006; Upstill-Goddard 2006). However, a direct comparison to the literature is only possible with more information about the experimental and in situ conditions (e.g., hydrodynamics, gas transfer velocity). Strongly increasing CH_4 fluxes were detected during the last GW phase, GW3 (from 16.5 to 77.3 $\mu mol\ m^{-2}\ d^{-1}$) indicating an unreached maximum of the CH_4 fluxes. On a global scale, enhanced hydrodynamic exchange with organic-rich sediments, such as those found in coastal wetlands and thawing coastal and subsea permafrost (especially in the northern hemisphere), might thus modulate coastal carbon dynamics in the framework of climate change and sea-level rise scenarios. Coastal erosion caused by sea-level rise can cause not only the loss of ecosystems, but also a shift in the carbon reservoir balance.

Conclusions and limitation

Coastal wetlands and carbon-rich deposits are found along a majority of the German Baltic Sea coast (Sterr 2008) and are abundant on every continent (Strack 2008). Thus, submerging of peatlands due to sea-level rise, subsidence as well as rewetting of drained coastal peatlands has potential to reshape the nearshore coastal fluxes of various environmentally important compounds in the future, creating a pressing need to understand the biogeochemical processes in these settings.

Specific to this study, we aimed to better understand the effect of salt water intrusion in the near-coast peat environments. We ran a controlled column experiment, which, although the method may have limited transferability to natural conditions, it is to date the most appropriate technique for the purposes of this research and reliable and field-comparable results can still be obtained. The experimental setup simulated coastal circulation conditions and represented a fragment of the complex in situ conditions along the study site. The 3-km-long coastline of the adjacent wetland of the study site is exposed to changing conditions leading to large variations in sediments and physicochemical conditions. However, the sediment cores investigated represent a larger area of the sedimentary conditions along the coastline (Kreuzburg et al. 2018).

The aims of the column experiment have been summarized in Fig. 8. The implications of our results for coastal zones illustrate: (1) the intrusion of SO_4^{2-}-containing SW through C_{org}-rich sediments of terrestrial origin (peat deposits), results in SO_4^{2-} reduction, with DIC as the end product. (2) The discharge of O_2-depleted GW triggered enhanced DOC release from the sediments and facilitated methanogenesis. The resulting release of CO_2 and CH_4 may represent a so far unnoticed source of coastal greenhouse gas emissions. Our results provide clear evidence of bioavailable DOC being produced from

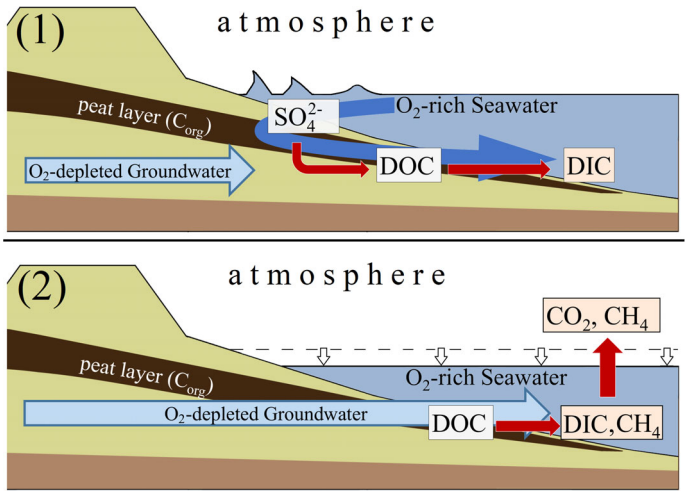

Fig. 8. Conceptual extraction of the carbon exchange processes in the submarine, peat-containing estuary along the shoreline of our study site with (1) elevated sea-level situation and wave setup. The blue arrow visualizes the intrusion of SW into carbon-rich sediments, the red arrows showing the mineralization pathway. The process includes DOC mineralization via SO_4^{2-} reduction resulting in a discharge of DIC. (2) Low sea-level situation and calm surface water conditions. The discharge of GW displaces methane oxidants (O_2, SO_4^{2-}), increases DOC release and facilitates CH_4 production and emission.

solid-phase C_{org} (of that peat) that had already been submerged for considerable lengths of time. The results also show that substrate, transport processes, redox conditions and salinity control peat degradation, DOC mobilization, and CO_2 and CH_4 release. Regarding the distribution of microbial, key players, we found that the abundance of the methanogens increased with increasing depth in the peat sediments and was not dependent on the abundance of the SRB. Thus, we conclude that the microbial activity is closely coupled with biodegradable organic carbon.

The experimental findings (particularly with the high spatial and temporal resolution of measurements) improve the understanding of biogeochemical processes of peat-derived carbon cycling and transformation. Sediments containing peat deposits can be hot spots of increased release of and mineralization of DOC and may play an important role in the release of climate relevant gases (CH_4, CO_2) in coastal zones. Ongoing coastal erosion and suspension of peat deposits and wetland loss due to sea-level rise and the frequency of storm events might promote the processes that have been investigated in this study. However, more detailed information about the hydrological cycles, geochemical properties, and solute concentrations is fundamental for process balancing and to justify comparisons with the field.

References

Aben, R. C., and others. 2017. Cross continental increase in methane ebullition under climate change. Nat. Commun. **8**: 1682. doi:10.1038/s41467-017-01535-y

Andersen, M. S., V. Nyvang, R. Jakobsen, and D. Postma. 2005. Geochemical processes and solute transport at the seawater/freshwater interface of a sandy aquifer. Geochim. Cosmochim. Acta **69**: 3979–3994. doi:10.1016/j.gca.2005.03.017

Anderson, T. F., and M. A. Arthur. 1983. Stable isotopes of oxygen and carbon and their application to sedimentologic and paleoenvironmental problems, p. 1.1–1.151. SEPM Society for Sedimentary Geology.

Aravena, R., and L. I. Wassenaar. 1993. Dissolved organic carbon and methane in a regional confined aquifer, southern Ontario, Canada: Carbon isotope evidence for associated subsurface sources. Appl. Geochem. **8**: 483–493. doi:10.1016/0883-2927(93)90077-T

Badocco, D., A. Mondin, and P. Pastore. 2012. Determination of thermodynamic parameters from light intensity signals obtained from oxygen optical sensors. Sens. Actuators B Chem. **163**: 165–170. doi:10.1016/j.snb.2012.01.030

Bange, H. W. 2006. Nitrous oxide and methane in European coastal waters. Estuar. Coast. Shelf Sci. **70**: 361–374. doi:10.1016/j.ecss.2006.05.042

Bange, H. W., U. H. Bartell, S. Rapsomanikis, and M. O. Andreae. 1994. Methane in the Baltic and North Seas and a reassessment of the marine emissions of methane. Global Biogeochem. Cycles **8**: 465–480. doi:10.1029/94GB02181

Barlow, P. M., and E. G. Reichard. 2010. Saltwater intrusion in coastal regions of North America. Hydrgeol. J. **18**: 247–260. doi:10.1007/s10040-009-0514-3

Bender, M. L., and D. T. Heggie. 1984. Fate of organic carbon reaching the deep sea floor: A status report. Geochim. Cosmochim. Acta **48**: 977–986. doi:10.1016/0016-7037(84)90189-3

Berry, D. F., L. W. Zelazny, and H. L. Walker. 1990. Aluminum and organic matter mobilization from forest soil infiltrated with acidified calcium sulfate solutions. Soil Sci. Soc. Am. J. **54**: 1757–1762. doi:10.2136/sssaj1990.03615995005400060042x

Bickert, T. 2000. Influence of geochemical processes on stable isotope distribution in marine sediments, p. 309–333. *In* H. D. Schulz and M. Zabel [eds.], Marine Geochemistry. Springer, Berlin Heidelberg.

Borges, A. V., W. Champenois, N. Gypens, B. Delille, and J. Harlay. 2016. Massive marine methane emissions from near-shore shallow coastal areas. Sci. Rep. **6**: 27908. doi:10.1038/srep27908

Boutton, T. W. 1991. Stable carbon isotope ratios of natural materials: II. Atmospheric, terrestrial, marine, and freshwater environments. In, D. C. Coleman and B. Fry [eds.], Carbon isotope techniques, p. 173–185. Academic Press. doi:10.1016/B978-0-12-179730-0.50016-3

Bugna, G. C., J. P. Chanton, J. E. Cable, W. C. Burnett, and P. H. Cable. 1996. The importance of groundwater discharge to the methane budgets of nearshore and continental shelf waters of the northeastern Gulf of Mexico. Geochim. Cosmochim. Acta **60**: 4735–4746. doi:10.1016/S0016-7037(96)00290-6

Burdige, W. C. 2011. 5.09—Estuarine and coastal sediments–coupled biogeochemical cycling. Treat. Estuar. Coast. Sci. **5**: 279–308. doi:10.1016/B978-0-12-374711-2.00511-8

Burnett, W. C., and others. 2006. Quantifying submarine groundwater discharge in the coastal zone via multiple methods. Sci. Total Environ. **367**: 498–543. doi:10.1016/j.scitotenv.2006.05.009

Bussmann, I., and E. Suess. 1998. Groundwater seepage in Eckernförde Bay (Western Baltic Sea): Effect on methane and salinity distribution of the water column. Cont. Shelf Res. **18**: 1795–1806. doi:10.1016/S0278-4343(98)00058-2

Cabrera, R. I. 1998. Monitoring chemical properties of container growing media with small soil solution samplers. The use of trade names in this publication does not imply endorsement of the products used or criticism of similar ones not used. Sci. Hortic. **75**: 113–119. doi:10.1016/S0304-4238(98)00121-6

Chambers, L. G., K. R. Reddy, and T. Z. Osborne. 2011. Short-term response of carbon cycling to salinity pulses in a freshwater wetland. Soil Sci. Soc. Am. J. **75**: 2000–2007. doi:10.2136/sssaj2011.0026

Chambers, L. G., S. E. Davis, T. Troxler, J. N. Boyer, A. Downey-Wall, and L. J. Scinto. 2014. Biogeochemical

effects of simulated sea level rise on carbon loss in an Everglades mangrove peat soil. Hydrobiologia **726**: 195–211. doi:10.1007/s10750-013-1764-6

Cicerone, R. J., and R. S. Oremland. 1988. Biogeochemical aspects of atmospheric methane Glob. Biogeochem. Cycles **2**: 299–327. doi:10.1029/GB002i004p00299

Cyberski, J. 2011. Climate, hydrology and hydrodynamics of the Baltic Sea. *In* S. Uścinowicz [ed.]. Geochemistry of Baltic Sea surface sediments, p. 55–65. Warszawa: Polish Geological Institute–National Research Institute.

Dahms, P. 1991. Studie Wasserregulierung Hütelmoor. Unveröffentlichte Studie des StAUN Rostock, doi:10.1111/j.1439-0450.1991.tb00915.x.

Dale, A. W., P. Regnier, N. J. Knab, B. B. Jørgensen, and P. Van Cappellen. 2008. Anaerobic oxidation of methane (AOM) in marine sediments from the Skagerrak (Denmark): II. Reaction-transport modeling. Geochim. Cosmochim. Acta **72**: 2880–2894. doi:10.1016/j.gca.2007.11.039

Dar, S. A., R. Kleerebezem, A. J. M. Stams, J. G. Kuenen, and G. Muyzer. 2008. Competition and coexistence of sulfate-reducing bacteria, acetogens and methanogens in a lab-scale anaerobic bioreactor as affected by changing substrate to sulfate ratio. Appl. Microbiol. Biotechnol. **78**: 1045–1055. doi:10.1007/s00253-008-1391-8

Delaune, R. D., J. A. Nyman, and W. H. Patrick. 1994. Peat collapse, ponding and wetland loss in a rapidly submerging coastal marsh. J. Coast. Res. **10**: 1021–1030.

Deppenmeier, U. 2002. The unique biochemistry of methanogenesis. Progr. Nucl. Acid Res. Mol. Biol. **71**: 223–283. doi:10.1016/S0079-6603(02)71045-3

Dillon, K. S., D. R. Corbett, J. P. Chanton, W. C. Burnett, and D. J. Furbish. 1999. The use of sulfur hexafluoride (SF_6) as a tracer of septic tank effluent in the Florida Keys. J. Hydrol. **220**: 129–140. doi:10.1016/S0022-1694(99)00073-6

EPA SOP for DOC. 2002. EPA standard operating procedure for dissolved organic carbon, LG211, Revision 03, December 2002. Available from http://www.epa.gov/greatlakes/monitoring/sop/chapter_2/LG211.pdf

Evans, C. D., and others. 2012. Acidity controls on dissolved organic carbon mobility in organic soils. Glob. Chang. Biol. **18**: 3317–3331. doi:10.1111/j.1365-2486.2012.02794.x

Freeman, C., C. D. Evans, D. T. Monteith, B. Reynolds, and N. Fenner. 2001. Export of organic carbon from peat soils. Nature **412**: 785. doi:10.1038/35090628

Gatland, J. R., I. R. Santos, D. T. Maher, T. M. Duncan, and D. V. Erler. 2014. Carbon dioxide and methane emissions from an artificially drained coastal wetland during a flood: Implications for wetland global warming potential. J. Geophys. Res. Biogeo. **119**: 1698–1716. doi:10.1002/2013JG002544

Gorham, E. 1995. The biogeochemistry of northern peatlands and its possible responses to global warming. In Biotic feedbacks in the global climate system: Will the warming feed the warming. p. 169–187. New York: Oxford University Press.

Gosch, L., M. Janssen, and B. Lennartz. 2018. Impact of the water salinity on the hydraulic conductivity of fen peat. Hydrol. Process. **32**: 1214–1222. doi:10.1002/hyp.11478

Gosch, L., H. Townsend, M. Kreuzburg, M. Janssen, F. Rezanezhad, and B. Lennartz. 2019. Sulfate mobility in fen peat and its impact on the release of solutes. Front. Environ. Sci. **7**: 189. doi:10.3389/fenvs.2019.00189

Hahn, J., S. Köhler, S. Glatzel, and G. Jurasinski. 2015. Methane exchange in a coastal fen in the first year after flooding—A systems shift. 1–25, doi:10.1167/tvst.4.4.1.

Henrichs, S. M., and W. S. Reeburgh. 1987. Anaerobic mineralization of marine sediment organic matter: Rates and the role of anaerobic processes in the oceanic carbon economy. Geomicrobiol. J. **5**: 191–237. doi:10.1080/01490458709385971

Heyer, J., and U. Berger. 2000. Methane emission from the coastal area in the southern Baltic Sea. Estuar. Coast. Shelf Sci. **51**: 13–30. doi:10.1006/ecss.2000.0616

Holmer, M., and E. Kristensen. 1994. Coexistence of sulfate reduction and methane production in an organic-rich sediment. Mar. Ecol. Prog. Ser. **107**: 177–184. doi:10.3354/meps107177

Hooijer, A., S. Page, J. Jauhiainen, W. A. Lee, X. X. Lu, A. Idris, and G. Anshari. 2012. Subsidence and carbon loss in drained tropical peatlands. Biogeosciences **9**: 1053–1071. doi:10.5194/bg-9-1053-2012

Hübner, E., and B. T. Gräff. 2013. Küstenhydrologie und -topografie im Naturschutzgebiet Hütelmoor.

IsoPrime. 2014. IsoPrime100 user's guide v1.02 for Ionvantage, 2014. Cheadle, UK. 219 p: IsoPrime Limited, Cheadle Hulme. doi:10.17226/21683

Iversen, N., and T. H. Blackburn. 1981. Seasonal rates of methane oxidation in anoxic marine sediments. Appl. Environ. Microbiol. **41**: 1295–1300. doi:10.1128/AEM.41.6.1295-1300.1981

Jørgensen, B. B., A. Weber, and J. Zopfi. 2001. Sulfate reduction and anaerobic methane oxidation in Black Sea sediments. Deep Sea Res. Part I **48**: 2097–2120. doi:10.1016/S0967-0637(01)00007-3

Joye, S. B., and J. T. Hollibaugh. 1995. Influence of sulfide inhibition of nitrification on nitrogen regeneration in sediments. Science **270**: 623–625. doi:10.1126/science.270.5236.623

Jurasinski, G., and others. 2018. Understanding the coastal ecocline: Assessing sea–land interactions at non-tidal, low-lying coasts through interdisciplinary research. Front. Mar. Sci. **5**: 342. doi:10.3389/fmars.2018.00342

Kalbitz, K., S. Solinger, J.-H. Park, B. Michalzik, and E. Matzner. 2000. Controls on the dynamics of dissolved organic matter in soils: A review. Soil Sci. **165**: 277–304. doi:10.1097/00010694-200004000-00001

Knee, K., J. H. Street, E. G. Grossman, and A. Paytan. 2010. Nutrient inputs to the coastal ocean from submarine

groundwater discharge in a groundwater-dominated system: Relation to land use (Kona coast, Hawaii, U.S.A.). Limnol. Oceanogr. **55**: 1105–1122. doi:10.4319/lo.2010.55.3.1105

Knee, K. L., and A. Paytan. 2012. Submarine groundwater discharge: A source of nutrients, metals, and pollutants to the Coastal Ocean. Elsevier. doi:10.1371/journal.pone.0047243

Knight, B. P., A. M. Chaudri, S. P. McGrath, and K. E. Giller. 1998. Determination of chemical availability of cadmium and zinc in soils using inert soil moisture samplers. Environ. Pollut. **99**: 293–298. doi:10.1016/S0269-7491(98)00021-9

Koch, S., G. Jurasinski, F. Koebsch, M. Koch, and S. Glatzel. 2014. Spatial variability of annual estimates of methane emissions in a *Phragmites australis* (cav.) trin. ex steud. dominated restored coastal brackish fen. Wetlands **34**: 593–602. doi:10.1007/s13157-014-0528-z

Koebsch, F., G. Jurasinski, M. Koch, J. Hofmann, and S. Glatzel. 2015. Controls for multi-scale temporal variation in ecosystem methane exchange during the growing season of a permanently inundated fen. Agric. For. Meteorol. **204**: 94–105. doi:10.1016/j.agrformet.2015.02.002

Koehler, A.-K., K. Murphy, G. Kiely, and M. Sottocornola. 2009. Seasonal variation of DOC concentration and annual loss of DOC from an Atlantic blanket bog in South Western Ireland. Biogeochemistry **95**: 231–242. doi:10.1007/s10533-009-9333-9

Kolp, O. 1957. Die nordöstliche Heide Mecklenburgs. VEB Deutscher Verlag Der Wis Enschaften.

Kotwicki, L., K. Grzelak, M. Czub, O. Dellwig, T. Gentz, B. Szymczycha, and M. E. Böttcher. 2014. Submarine groundwater discharge to the Baltic coastal zone: Impacts on the meiofaunal community. J. Mar. Syst. **129**: 118–126. doi:10.1016/j.jmarsys.2013.06.009

Kreuzburg, M., M. Ibenthal, M. Janssen, G. Rehder, M. Voss, M. Naumann, and P. Feldens. 2018. Sub-marine continuation of peat deposits from a coastal peatland in the Southern Baltic Sea and its Holocene development. Front. Earth Sci. **6**: 103. doi:10.3389/feart.2018.00103

Küsel, K., M. Blöthe, D. Schulz, M. Reiche, and H. L. Drake. 2008. Microbial reduction of iron and porewater biogeochemistry in acidic peatlands. Biogeosciences **5**: 1537–1549. doi:10.5194/bg-5-1537-2008

Larsen, M., S. M. Borisov, B. Grunwald, I. Klimant, and R. N. Glud. 2011. A simple and inexpensive high resolution color ratiometric planar optode imaging approach: application to oxygen and pH sensing: A simple RGB based planar optode imaging approach. Limnol. Oceanogr. Methods **9**: 348–360. doi:10.4319/lom.2011.9.348

Lasak, S., J. Hahn, G. Jurasinski, S. Köhler, and S. Glatzel. 2010. Methanfreisetzungen im Rahmen des Auftauens eines überfluteten Küstenmoors. *In* K. Kaiser, J. Libra, B. Merz, O. Bens, and R. F. Hüttl. [Hrsg.], Aktuelle Probleme im Wasserhaushalt von Nordostdeutschland: Trends, Ursachen, Lösungen. Scientific Technical Report 10/10, p. 129–132. Deutsches GeoForschungsZentrum, Potsdam.

Li, L., D. A. Barry, F. Stagnitti, and J. Y. Parlange. 1999. Submarine groundwater discharge and associated chemical input to a coastal sea. Water Resour. Res. **35**: 3253–3259. doi:10.1029/1999WR900189

Limpens, J., and others. 2008. Peatlands and the carbon cycle: From local processes to global implications-a synthesis. Biogeosciences **5**: 1475–1491. doi:10.5194/bg-5-1475-2008

Liu, D. Y., W. X. Ding, Z. J. Jia, and Z. C. Cai. 2011. Relation between methanogenic archaea and methane production potential in selected natural wetland ecosystems across China. Biogeosciences **8**: 329–338. doi:10.5194/bg-8-329-2011

Luo, M., J.-F. Huang, W.-F. Zhu, and C. Tong. 2017. Impacts of increasing salinity and inundation on rates and pathways of organic carbon mineralization in tidal wetlands: A review. Hydrobiologia, pp 31–49.

Lyman, J. 1969. Redefinition of salinity and chlorinity. Limnol. Oceanogr. **14**: 928–929. doi:10.4319/lo.1969.14.6.0928

Meyers, P. A. 1997. Organic geochemical proxies of paleoceanographic, paleolimnologic, and paleoclimatic processes. Org. Geochem. **27**: 213–250. doi:10.1016/S0146-6380(97)00049-1

Miegel, K., T. Graeff, B. Selle, T. Salzmann, C. Franck, and A. Bronstert. 2016. Untersuchung eines renaturierten Niedermoores an der mecklenburgischen Ostseeküste—Teil I: Systembeschreibung und hydrologische Grundcharakterisierung. HyWa **10**: 5675. doi:10.5675/HyWa_2016,4_1

Moore, T. R., and M. Dalva. 1993. The influence of temperature and water-table position on carbon-dioxide and methane emissions from laboratory columns of peatland soils. J. Soil Sci. **44**: 651–664. doi:10.1111/j.1365-2389.1993.tb02330.x

Moore, W. S. 1999. The subterranean estuary: A reaction zone of ground water and sea water. Mar. Chem. **65**: 111–125. doi:10.1016/S0304-4203(99)00014-6

Moore, W. S. 2010. The effect of submarine groundwater discharge on the ocean. Ann. Rev. Mar. Sci. **2**: 59–88. doi:10.1146/annurev-marine-120308-081019

Mulholland, P. J. 1981. Formation of particulate organic carbon in water from a southeastern swamp-stream. Limnol. Oceanogr. **26**: 790–795. doi:10.4319/lo.1981.26.4.0790

Mulholland, P. J. 2003. Large-scale patterns in dissolved organic carbon concentration, flux, and sources, p. 139–159. *In* S. E. G. Findlay and R. L. Sinsabaugh [eds.], Aquatic ecosystems. Academic Press. doi:10.1016/B978-012256371-3/50007-X

Neubauer, S. C. 2013. Ecosystem responses of a tidal freshwater marsh experiencing saltwater intrusion and altered

hydrology. Estuaries Coasts **36**: 491–507. doi:10.1007/s12237-011-9455-x

Nicholls, R. J., and A. Cazenave. 2010. Sea-level rise and its impact on coastal zones. Science **328**: 1517–1520. doi:10.1126/science.1185782

Nieuwenhuis, H. S., and F. Schokking. 1997. Land subsidence in drained peat areas of the Province of Friesland, The Netherlands. Q. J. Eng. Geol. Hydrogeol. **30**: 37–48. doi:10.1144/GSL.QJEGH.1997.030.P1.04

Nieuwenhuize, J., Y. E. M. Maas, and J. J. Middelburg. 1994. Rapid analysis of organic carbon and nitrogen in particulate materials. Mar. Chem. **45**: 217–224. doi:10.1016/0304-4203(94)90005-1

Ostrovsky, I. 2003. Methane bubbles in Lake Kinneret: Quantification and temporal and spatial heterogeneity. Limnol. Oceanogr. **48**: 1030–1036. doi:10.4319/lo.2003.48.3.1030

Ozuolmez, D., H. Na, M. A. Lever, K. U. Kjeldsen, B. B. Jørgensen, and C. M. Plugge. 2015. Methanogenic archaea and sulfate reducing bacteria co-cultured on acetate: Teamwork or coexistence? Front. Microbiol. **6**: 492. doi:10.3389/fmicb.2015.00492

Peltonen, K. 2002. Direct groundwater inflow to the Baltic Sea, Nordic Council of Ministers. TemaNord, **2002**: 503. doi:10.1208/pt030432

Plag, H.-P., and S. Jules-Plag. 2013. Sea-level rise and coastal ecosystems, Elsevier. **4**: 163–184.

Plaut, Z., M. Edelstein, and M. Ben-Hur. 2013. Overcoming salinity barriers to crop production using traditional methods. Critic. Rev. Plant Sci. **32**: 250–291. doi:10.1080/07352689.2012.752236

Porubsky, W. P., N. B. Weston, W. S. Moore, C. Ruppel, and S. B. Joye. 2013. Dynamics of submarine groundwater discharge and associated fluxes of dis- solved nutrients, carbon, and trace gases to the coastal zone (Okatee River estuary, South Carolina). Geochim. Cosmochim. Acta **131**: 81–97. doi:10.1016/j.gca.2013.12.030

Ramaswamy, V., and others. 2001. Radiative forcing of climate change. *In* J. T. Houghton, Y. Ding, D. J. Griggs, M. Noguer, P. J. van der Linden, X. Dai, K. Maskell and C. A. Johnson [eds.], Climate change 2001: The scientific basis. Contribution of working group I to the third assessment report of the intergovernmental panel on climate change, p. 349–416. Cambridge, UK: Cambridge University Press.

Rapaglia, J. 2005. Submarine groundwater discharge into Venice Lagoon, Italy. Estuaries **28**: 705–713. doi:10.1007/BF02732909

Rasband, W.S. 2015. ImageJ: US National Institutes of Health. Bethesda, MD. Available from http://imagej.nih.gov/ij, doi:10.1101/cshperspect.a020495.

Reeburgh, W. S. 1980. Anaerobic methane oxidation: Rate depth distributions in Skan Bay sediments. Earth Planet. Sci. Lett. **47**: 345–352. doi:10.1016/0012-821X(80)90021-7

Reeburgh, W. S., and M. J. Alperin. 1988. Studies on anaerobic methane oxidation. SCOPE/UNEP **66**: 367–375.

Rezanezhad, F., R. M. Couture, R. Kovac, D. O'Connell, and P. Van Cappellen. 2014. Water table fluctuations and soil biogeochemistry: An experimental approach using an automated soil column system. J. Hydrol. **509**: 245–256. doi:10.1016/j.jhydrol.2013.11.036

Rezanezhad, F., J. S. Price, W. L. Quinton, B. Lennartz, T. Milojevic, and P. Van Cappellen. 2016. Structure of peat soils and implications for water storage, flow and solute transport: A review update for geochemists. Chem. Geol. **429**: 75–84. doi:10.1016/j.chemgeo.2016.03.010

Robinson, C., L. Li, and D. A. Barry. 2007. Effect of tidal forcing on a subterranean estuary. Adv. Water Resour. **30**: 851–865. doi:10.1016/j.advwatres.2006.07.006

Roulet, N., T. Moore, J. Bubier, and P. Lafleur. 1992. Northern fens: Methane flux and climatic change. Tellus B Chem. Phys. Meteorol. **44B**: 100–105.

Santos, I. R., B. D. Eyre, and M. Huettel. 2012. The driving forces of porewater and groundwater flow in permeable coastal sediments: A review. Estuar. Coast. Shelf Sci. **98**: 1–15. doi:10.1016/j.ecss.2011.10.024

Säurich, A., B. Tiemeyer, U. Dettmann, and A. Don. 2019. How do sand addition, soil moisture and nutrient status influence greenhouse gas fluxes from drained organic soils? Soil Biol. Biogeochem. **135**: 71–84. doi:10.1016/j.soilbio.2019.04.013

Schlüter, M., E. J. Sauter, C. E. Andersen, H. Dahlgaard, and P. R. Dando. 2004. Spatial distribution and budget for submarine groundwater discharge in Eckernförde Bay (Western Baltic Sea). Limnol. Oceanogr. **49**: 157–167. doi:10.4319/lo.2004.49.1.0157

Seeberg-Elverfeldt, J., M. Schlüter, T. Feseker, and M. Kölling. 2005. Rhizon sampling of porewaters near the sediment-water interface of aquatic systems. Limnol. Oceanogr. Methods **3**: 361–371. doi:10.4319/lom.2005.3.361

Seitzinger, S. P., and J. A. Harrison. 2008. Land-based nitrogen sources and their delivery to coastal systems. doi:10.1016/B978-0-12-372522-6.00009-8

Sela-Adler, M., Z. Ronen, B. Herut, G. Antler, H. Vigderovich, W. Eckert, and O. Sivan. 2017. Co-existence of methanogenesis and sulfate reduction with common substrates in sulfate-rich estuarine sediments. Front. Microbiol. **8**: 766. doi:10.3389/fmicb.2017.00766

Sergeev, A., V. Sivkov, V. Zhamoida, D. Ryabchuk, A. Bitinas, and J. Mažeika. 2015. Holocene biogenic sediments of the Curonian Spit (south-eastern Baltic Sea coast). Baltica **28**: 41–50. doi:10.5200/baltica.2015.28.05

Sirin, A., and J. Laine. 2008. Peatlands and greenhouse gases. *In* F. Parish, et al. [eds.], Assesment on peatlands, biodiversity and climate change: main report, p. 118–138. Global Environment Center, Kuala Lumpur.

Slomp, C. P., and P. Van Cappellen. 2004. Nutrient inputs to the coastal ocean through submarine groundwater

discharge: Controls and potential impact. J. Hydrol. **295**: 64–86. doi:10.1016/j.jhydrol.2004.02.018

Stadtman, T. C., and H. A. Barker. 1949. Studies on the methane fermentation; tracer experiments on the mechanism of methane formation. Arch. Biochem. **21**: 256–264.

Steinton, M. P., M. J. Capel, and F. A. J. Armstrong. 1977. Chemical analysis of fresh water, 2nd Ed. Misc. Spec. Publ. Dept. Environment Canada 25. pp 166.

Stein, R. 1991. Accumulation of organic carbon in Baffin Bay and Labrador Sea sediments (ODP-Leg 105). In Accumulation of organic carbon in marine sediments: Results from the Deep Sea Drilling Project/Ocean Drilling Program (DSDP/ODP), p. 40–84. Heidelberg: Springer Berlin. doi:10.1007/BFb0010387

Sterr, H. 2008. Assessment of vulnerability and adaptation to sea-level rise for the coastal zone of Germany. J. Coast. Res. **24**: 380–393. doi:10.2112/07A-0011.1

St-Jean, G. 2003. Automated quantitative and isotopic (13C) analysis of dissolved inorganic carbon and dissolved organic carbon in continuous-flow using a total organic carbon analyser. Rapid Commun. Mass Spectrom. **17**: 419–428. doi:10.1002/rcm.926

Stocker, T. F., and others. 2013. Climate change 2013: The physical science basis. *In* Contribution of working group I to the fifth assessment report of the Intergovernmental Panel on Climate Change 2013. Cambridge University Press. doi:10.1136/bmjspcare-2012-000406

Strack, M. 2008. Peatlands and climate change. International Peat Society.

Strehse, R., H. Bohne, Y. Amha, and P. Leinweber. 2018. The influence of salt on dissolved organic matter from peat soils. Org. Geochem. **125**: 270–276. doi:10.1016/j.orggeochem.2018.10.001

Taffs, K. H., B. Logan, J. F. Parr, and G. E. Jacobsen. 2012. The evolution of a coastal peatland at Byron Bay, Australia: multi-proxy evidence from the microfossil record. *In* S. G. Haberle, and B. David (eds), Terra Australis 34: peopled landscapes: archaeological and biogeographic approaches to landscapes, ANU E-press, Canberra, ACT, Australia, pp. 429–442.

Tiemeyer, B., N. Pfaffner, S. Frank, K. Kaiser, and S. Fiedler. 2017. Pore water velocity and ionic strength effects on DOC release from peat-sand mixtures: Results from laboratory and field experiments. Geoderma **296**: 86–97. doi:10.1016/j.geoderma.2017.02.024

Tipping, E., and M. A. Hurley. 1988. A model of solid-solution interactions in acid organic soils, based on the complexation properties of humic substances. Eur. J. Soil Sci. **39**: 509–519.

Upstill-Goddard, R. C. 2006. Air–sea gas exchange in the coastal zone. Estuar. Coast. Shelf Sci. **70**: 388–404. doi:10.1016/j.ecss.2006.05.043

Voigtländer, U., J. Schmidt, W. Scheller. 1996. Pflege-und Entwicklungsplan NSG Heiligensee und Hütelmoor, doi:10.1103/PhysRevLett.77.3861.

von Post, L. 1922. Sveriges Geologiska Undersöknings torvinventering och några av dess hittills vunna resultat. Sver. Geo. Unders.

Vuillemin, A., and others. 2018. Metabolic potential of microbial communities from ferruginous sediments. Environ. Microbiol. **20**: 4297–4313. doi:10.1111/1462-2920.14343

Wang, H., C. J. Richardson, M. Ho, and N. Flanagan. 2016. Drained coastal peatlands: A potential nitrogen source to marine ecosystems under prolonged drought and heavy storm events—A microcosm experiment. Sci. Total Environ. **566–567**: 621–626.

Weber, T., N. A. Wiseman, and A. Kock. 2019. Global ocean methane emissions dominated by shallow coastal waters. Nat. Commun. **10**: 4586. doi:10.1038/s41467-019-12541-7

Wen, X., and others. 2018. Predominance of methanogens over methanotrophs in rewetted fens characterized by high methane emissions. Biogeosiences **15**: 6519–6536. doi: https://doi.org/10.5194/bg-15-6519-2018

Wen, Y., E. S. Bernhardt, W. Liu, J. Yan, E. M. Baruch, and C. M. Bergmann. 2018. Salt effects on carbon mineralization in southern coastal wetland soils of the United States. Geoderma **339**: 31–39. doi:10.1016/j.geoderma.2018.12.035

Weston, N. B., M. A. Vile, S. C. Neubauer, and D. J. Velinsky. 2011. Accelerated microbial organic matter mineralization following salt-water intrusion into tidal freshwater marsh soils. Biogeochemistry **102**: 135–151. doi:10.1007/s10533-010-9427-4

Whiticar, M. J. 2002. Diagenetic relationships of methanogenesis, nutrients, acoustic turbidity, pockmarks and freshwater seepages in Eckernförde Bay. Mar. Geol. **182**: 29–53. doi:10.1016/S0025-3227(01)00227-4

Whiticar, M. J., E. Faber, and M. Schoell. 1986. Biogenic methane formation in marine and freshwater environments: CO_2 reduction vs. acetate fermentation—Isotope evidence. Geochim. Cosmochim. Acta Theriol. **50**: 693–709. doi:10.1016/0016-7037(86)90346-7

van Winden, J. F., G.-J. Reichart, N. P. McNamara, A. Benthien, and J. S. S. Damsté. 2012. Temperature-induced increase in methane release from peat bogs: A mesocosm experiment. PLoS One **7**: e39614. doi:10.1371/journal.pone.0039614

Zauft, M., H. Fell, F. Glaßer, N. Rosskopf, and J. Zeitz. 2010. Carbon storage in the peatlands of Mecklenburg-Western Pomerania, north-east Germany. Mires & Peat **6**: 1–12.

Zehnder, A. J. B., and R. Mitchell. 1978. Ecology of methane formation. Water Pollut. Microbiol. **2**: 349–376.

Zhang, B., H. Tian, C. Lu, G. Chen, S. Pan, C. Anderson, and B. Poulter. 2017. Methane emissions from global wetlands: An assessment of the uncertainty associated with various wetland extent data sets. Atmos. Environ. **165**: 310–321. doi:10.1016/j.atmosenv.2017.07.001

Acknowledgments

We thank the editor, Dave Hambright, all associate editors, and three anonymous reviewers for their constructive valuable comments on the manuscript. We think that the reviewers' constructive comments were helpful in improving the clarity of the manuscript. This study was conducted within the framework of the Research Training Group "Baltic TRANSCOAST" funded by the Deutsche Forschungsgemeinschaft (DFG) under grant number GRK 2000 (https://www.baltic-transcoast.uni-rostock.de/). This is Baltic TRANSCOAST publication no. GRK2000/0031. We thank our colleagues from the GRK "Baltic TRANSCOAST" as well as Iris Liskow (IOW), who carried out geochemical analyses on the investigated sediments. This study was supported by the Helmholtz Gemeinschaft (HGF) funding the Terrestrial Environmental Observatories (TERENO) Network and the Helmholtz Young Investigators Group of S.L. (VH-NG-919). We are grateful to Marianne Vandergriendt (Ecohydrology Research Group, University of Waterloo, Canada for the great support on aqueous sample analyses and Sierra Willow Cranmer-Smith as well as Anke Saborowski for lab support. Furthermore, we thank Richard Heemskerk and Humam Mugammar, Environmental Isotope Laboratory, Waterloo, Canada for isotopic analyses on pore water samples.

Conflict of Interest

The authors have declared no conflicts of interest.

Submitted 01 April 2019
Revised 13 December 2019
Accepted 06 February 2020

Associate editor: Leila Hamdan